LRP 503/94 September 1994

Invited and Contributed Papers
presented at the

Joint Varenna-Lausanne International Workshop on "Theory of Fusion Plasmas" Varenna, Italy, August 22 - 26, 1994

by the Theory Group

LIST OF CONTENTS

		Page
-	THEORETICAL ASPECTS OF EFFECTS OF HIGH-ENERGY PARTICLES ON MHD MODES Invited Paper by *L. Villard, S. Brunner, J. Vaclavik*	1
-	NONLINEAR INTERACTION OF LOWER HYBRID WAVES *C. Bruderer, J. Vaclavik, K. Appert*	17
-	A KINETIC MODEL FOR THE GLOBAL POWER TRANSFER BETWEEN PARTICLES AND MHD WAVES *S. Brunner, L. Villard, J. Vaclavik*	25
-	LINEAR WAVE PROPAGATION IN RESISTIVE/HOT TOKAMAK PLASMAS *A. Jaun, K. Appert, H. Lütjens, J. Vaclavik, L. Villard*	31
-	3-D FOKKER-PLANCK CODE VALID FOR ARBITRARY COLLISIONALITY AND ADJOINT FUNCTION FOR BOOTSTRAP CURRENT CALCULATION *O. Sauter, Y.R. Lin-Liu, F.L. Hinton, J. Vaclavik*	41

LIST OF CONTENTS

		Page
-	THEORETICAL ASPECTS OF EFFECTS OF HIGH-ENERGY PARTICLES ON MHD MODES Invited Paper by *L. Villard, S. Brunner, J. Vaclavik*	1
-	NONLINEAR INTERACTION OF LOWER HYBRID WAVES *C. Bruderer, J. Vaclavik, K. Appert*	17
-	A KINETIC MODEL FOR THE GLOBAL POWER TRANSFER BETWEEN PARTICLES AND MHD WAVES *S. Brunner, L. Villard, J. Vaclavik*	25
-	LINEAR WAVE PROPAGATION IN RESISTIVE/HOT TOKAMAK PLASMAS *A. Jaun, K. Appert, H. Lütjens, J. Vaclavik, L. Villard*	31
-	3-D FOKKER-PLANCK CODE VALID FOR ARBITRARY COLLISIONALITY AND ADJOINT FUNCTION FOR BOOTSTRAP CURRENT CALCULATION *O. Sauter, Y.R. Lin-Liu, F.L. Hinton, J. Vaclavik*	41

Theoretical aspects of effects of high-energy particles on MHD modes

L.Villard, S.Brunner and J. Vaclavik

Centre de Recherches en Physique des Plasmas
Association Euratom - Confédération Suisse
Ecole Polytechnique Fédérale de Lausanne
21, av. des Bains – CH-1007 Lausanne/Switzerland

1 Introduction

The destabilization of Toroidicity-Induced Alfvén Eigenmodes (TAEs) [1] by fast particles in tokamak plasmas has been demonstrated both theoretically [2]-[6] and experimentally [7]-[9] . In the context of fusion-oriented research one should be able to predict as accurately as possible the conditions that can lead to such instabilities and to determine whether the region in parameter space where instabilities are avoided is compatible with the operation of a tokamak reactor. The expected density profile of fusion alpha particles in such a device is largely unknown and can only be inferred from theoretical models based on a number of assumptions on transport properties of plasmas yet to be produced. The instability threshhold strongly depends on this profile, therefore we must address the question of TAE stability for a wide range of fast particle density profiles and subsequently examine the compatibility with a fusion plasma.

Experiments in which the fast particles were produced by intense NBI heating [7]-[9] have shown that driving TAEs unstable can lead to rapid losses (bursts) of a substantial fraction of the fast particles. Although it is not sure that it would be the case for fusion alphas in a reactor, it is generally admitted that TAE instability should be avoided.

The possibility of exciting TAEs when they are stable is currently investigated at JET. The saddle coils now installed in the machine serve as antennas. The planned experiments aim at determining the spectrum of TAEs and their overall linear damping-growth rate by diagnosing the plasma response. Even in the absence of fast particles these experiments will be helpful in studying the damping mechanisms acting on TAEs.

From local theories [2]-[5] we know that three basic conditions must be met for instability:

1 The birth velocity v_0 of fast particles must exceed the parallel phase velocity v_p of the eigenmode so that the fast particles can resonantly interact with the eigenmode.

2 The fast particle pressure gradient $|dp_f/dr|$ must exceed a given threshhold so that the drift frequency ω^* is larger than the eigenfrequency ω_0 .

3 The fast particle induced growth-rate, $|\gamma/\omega|_{fast}$, must exceed the sum of all damping rates, $|\gamma/\omega|_{damp}$, due to the presence of the background plasma.

The damping mechanisms contributing to $|\gamma/\omega|_{damp}$ considered in our model are :

a) resonance absorption (sometimes called "continuum damping"), when the TAE eigenfrequency matches a frequency of the Alfvén continuum;

b) electron and ion Landau dampings due to the curvature drift and finite parallel electric field;

c) transit-time magnetic pumping (TTMP) on electrons and ions due to finite parallel magnetic field of the wave (compressibility).

In addition to these dampings the non-perturbative interaction with the kinetic Alfvén wave has been investigated in Ref. [10] . It is not considered in this paper.

Local theories suffer from a number of shortcomings. First, the TAEs are not localized at a given rational $q = (|m|+1/2)/|n|$ surface. They extend over the whole plasma cross-section, with wavefield components (e.g. the normal electric field) peaking at all such rational surfaces and other components (e.g. the poloidal electric field) having a broader radial dependence [11] . Second, the eigenfrequencies and eigenmode structures depend on global geometrical parameters (shape of the cross-section) and equilibrium profiles (density and q profiles). Third, local theories usually use some kind of expansion in geometrical parameters (a/R_0). A more accurate evaluation is needed in order to model actual and future tokamaks.

In this paper we adopt a global approach similar to that of Ref. [6] . The TAEs are computed globally in true toroidal geometry consistent with an ideal MHD equilibrium. Kinetic effects (damping and driving mechanisms) and fast particles are treated perturbatively. More precisely, we first obtain the global eigenmodes and then use these given eigenmode fields to evaluate the global overall wave-particle power transfer assuming given fast particle density profiles. The marginal stability point is obtained by scaling the number of fast particles so that the overall power transfer is zero. The wave-particle power transfers (to the electrons, bulk ions and fast ions) are evaluated using the drift-kinetic equations (DKE).

The paper is structured as follows. In the next section, the plasma model in toroidal geometry is briefly presented. The expressions for the DKE powers are derived for the various species (electrons, bulk ions and fast ions) in the companion paper in these proceedings [13] . In section 3 we show the results of our model applied to a wide variety of plasma parameters. In particular, the critical volume-averaged fast particle beta corresponding to marginal stability, $< \beta_f >_{cr}$, is calculated for a wide range of bulk plasma parameters ($v_0/v_{A0}, < \beta >, \omega/\omega_{ci}$) and fast particle profile widths ($s_{1/2}$). We discuss the results in section 4 and draw some conclusions in section 5.

2 Model

We consider ideal MHD axisymmetric equilibria $\vec{B}_0 = T\nabla\varphi + \nabla\varphi \times \nabla\psi$ where T is the toroidal flux function, φ is the toroidal angle and the poloidal flux ψ is a solution of the Grad-Shafranov equation obtained with the bicubic finite element code CHEASE [12] . The plasma is modelled as a cold, current-carrying plasma [14] neglecting electron inertia. In the limit $\omega/\omega_{ci} \rightarrow 0$ it is equivalent to ideal MHD setting the adiabaticity index to zero. The linearized equations for the electric wave field are written in the variational form :

$$\int_{V_p} \left\{ \left| \nabla \times \vec{E} - \vec{J}\, E_b \right|^2 - 2\, \vec{J} \cdot \nabla_{\|}\, \vec{e}_n\, |E_b|^2 - \frac{\omega^2}{c^2}\, \vec{E}^* \cdot \begin{pmatrix} \epsilon_{nn} & \epsilon_{nb} \\ \epsilon_{bn} & \epsilon_{bb} \end{pmatrix} \cdot \vec{E} \right\} d^3x + \int_{V_v} \left| \nabla \times \vec{E} \right|^2 d^3x = 0 \qquad (1)$$

where $\vec{e}_n = \nabla\psi/|\nabla\psi|$, $\vec{e}_{\|} = \vec{B}_0 / B_0$, $\vec{e}_b = \vec{e}_{\|} \times \vec{e}_n$, $\vec{J} = (\mu_0\, \vec{j_0} \times \vec{e_n})/B_0$, $\vec{j_0}$ is the equilibrium current, V_p is the plasma volume and

$$\begin{aligned} \epsilon_{nn} = \epsilon_{bb} &= \frac{c^2}{v_A^2} \sum_i \frac{f_i}{1 - (\frac{\omega}{\omega_{ci}})^2}, \\ \epsilon_{nb} = \epsilon_{bn}^* &= i \frac{c^2}{v_A^2} \sum_i \frac{f_i \omega/\omega_{ci}}{1 - (\frac{\omega}{\omega_{ci}})^2}, \\ f_i &= \frac{n_i m_i}{\sum_j n_j m_j}. \end{aligned} \qquad (2)$$

The plasma is surrounded by a vacuum region V_v enclosed by a perfectly conducting wall. In the vacuum region an antenna is modelled by an infinitely thin sheet $D(\vec{x})$ on which currents $\vec{j_a}$ of given frequency ω and toroidal mode number n are prescribed :

$$\vec{j_a} = \delta(D) \nabla D \times \nabla \alpha \qquad (3)$$

$$\alpha = \sum_n \alpha_n(\theta) \exp i(n\varphi - \omega t) \qquad (4)$$

where θ is the poloidal angle. The coefficients α_n are obtained from the Fourier series decomposition of the actual antenna currents. In this paper we consider the top saddle coil antennas that are installed in JET. Different phasings of the saddle coil currents give different toroidal Fourier spectra α_n. It is thus possible to select the desired mode number n (mainly $n = 1$ or $n = 2$).

Special care must be taken because of the existence of the Alfvén continuous spectrum. First, the solutions of Eq.(1) are singular at the magnetic surfaces where the antenna frequency matches that of a continuum. Consequently the wave is resonantly absorbed there, a process sometimes called "continuum damping". We solve the problem by adding a small imaginary part to the dielectric tensor in Eq.(1): ω is replaced by $\omega(1 + i\nu)$, with $\nu > 0$ to ensure causality. The operator in Eq.(1) is now regular but has lost its hermiticity. The limit $\nu \to 0$ is extrapolated from the numerical results of the LION code and gives a finite damping rate if the wave frequency is in the Alfvén continuum. Second, the discretization scheme must avoid spectral pollution. The use of hybrid elements in the LION code ensures that [11] [14] .

The variational form (1) is written in toroidal axisymmetric geometry using a toroidal magnetic coordinate system (ψ, χ, φ) where χ is a general poloidal coordinate, and discretized with finite hybrid elements in the plasma domain. The vacuum, including the antenna, is solved with a Green's function technique. The LION code computes the wavefield solution of Eq.(1) and the total absorbed power P for given antenna frequencies ω. A global mode shows as a peak on $P(\omega)$ [11] .

We know from kinetic theory in 1-D [15] that the inclusion of finite Larmor radius effects (FLR) usually does not modify the overall plasma power absorption but drastically

changes the wavefields near the former Alfvén resonances : mode conversion to the Kinetic Alfvén Wave (KAW) or to the Surface Quasi-Electrostatic Wave (SQEW) takes place. Therefore this paper is concerned with TAEs that have no continuum damping. Such cases arise when the profile of $1/q\sqrt{\rho}$ is rather flat (q is the safety factor and ρ is the mass density) thus aligning the $q = (|m| + 1/2)/|n|$ gaps. Continuum damping of low n modes was extensively studied in Ref [11] for a wide variety of shapes and profiles. High n cases were analytically studied in Refs [16] [17] . Only for cases where the profile $1/q\sqrt{\rho}$ is sufficiently peaked or hollow do the continuum gaps not overlap and one is sure to have continuum damping. Otherwise we can have TAEs "threading" the gaps and thus exactly zero continuum damping. It is safer to examine these cases since one cannot be sure to exclude them in a reactor (neither the density nor the q profile are easily controllable).

Considering the possible destabilization of TAEs by fast ions, marginal stability is reached when the sum of the DKE powers [13] of the different species $P_{species}$ is zero. For a given TAE, a given $n_f(s)$ profile shape and given $T_e(s)$ and $T_i(s)$ profiles, both P_f^{homo} and P_f^{inhomo} are proportional to the number of fast particles, or equivalently to the fast particle central density $n_f(0)$. The procedure to obtain the value $n_f(0)_{crit}$ corresponding to the marginal stability of a given TAE is the following: P_e, P_i, P_f^{homo} and P_f^{inhomo} are computed for given $T_e(s)$ and $T_i(s)$ and for a given $n_f(s)$ profile shape with an arbitrary value of $n_f(0)$. We have then

$$n_f(0)_{crit} = -\frac{P_e + P_i}{P_f^{homo} + P_f^{inhomo}} n_f(0). \tag{5}$$

From this value of $n_f(0)_{crit}$ and the given profiles $n_f(s)$ and $T_e(s)$ we compute the corresponding critical central fast particle beta $\beta_f(0)_{crit}$ and volume-averaged $< \beta_f >_{crit}$. We note that $n_f(0)_{crit} < 0$ means that the mode is always stable (i.e. stable for any fast particle density). Thus instead of the necessary instability criterion of local theories, $\omega - \omega^* < 0$, we have the necessary global instability criterion $P_f^{homo} + P_f^{inhomo} < 0$.

3 Results

3.1 Excitation of gap modes with JET saddle coils

We consider an up-down asymmetric equilibrium configuration representative of a "single-null" discharge in JET. The parameters are: $a/R_0 = 0.36$, $\kappa = 1.65$, $q_0 = 1.1$, $q_a = 3.34$, $p'(\psi) = 2/3$ of ballooning optimized $p'(\psi)$ profile, $I_p = 5MA$, $< \beta >= 3.9\%$, $\beta_{pol} = 0.78$. In all the equilibria considered in this paper we keep the same shape of cross-section, value of q_0 and $I^*(\psi)$ profile, where I^* is the magnetic-surface-averaged toroidal current density. Different equilibria are obtained by scaling the $p'(\psi)$ profile.

We first evaluate the plasma response to the antenna excitation at various frequencies in the absence of kinetic effects. Fig.1 shows the antenna coupling resistance vs frequency for the case $< \beta >= 3.9\%$ and for two different possible antenna phasings. Note that for standard JET parameters $R_0 = 3m$, $B_0 = 3.45T$, $n_{D0} = 5 \times 10^{19} m^{-3}$ a normalized frequency $R_0\omega/v_{A0}$ of unity corresponds to a frequency $f = 400kHz$. The dotted line corresponds to two top antennas at opposite toroidal locations with opposite phasings, exciting mainly $n = 1$ modes. The continuous line corresponds to all four top antennas

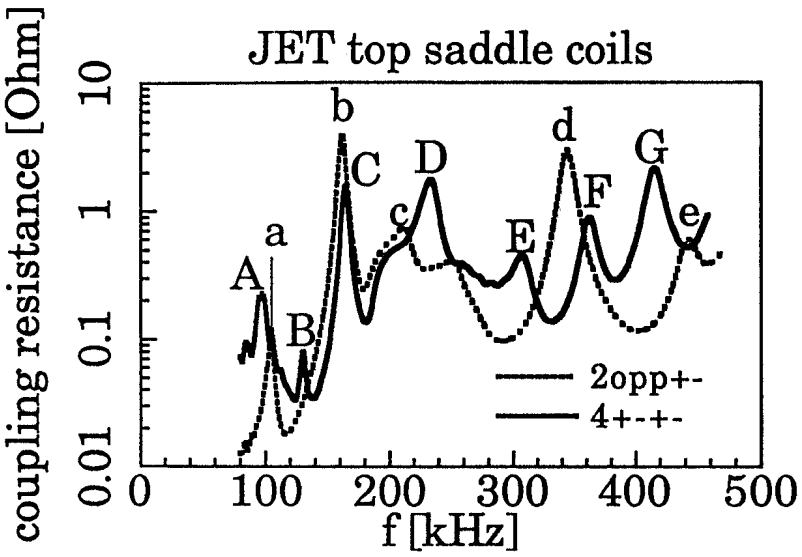

Fig.1. JET saddle coils resistive coupling versus frequency for two possible antenna phasings: two top antennas with (+,-) phasings (dotted line) and four top antennas with (+,-,+,-) phasings. The labels a,b,c,d,e correspond to $n = 1$ modes and A,B,C,D,E,F,G to $n = 2$ modes. The plasma parameters are $R_0 = 3m$, $B_0 = 3.45T$, $n_{D0} = 5 \times 10^{19} m^{-3}$, $\nu = 10^{-2}$, $q_0 = 1.1$, $q_a = 3.34$, $I_p = 5MA$, $< \beta >= 3.9\%$, $\beta_{pol} = 0.78$.

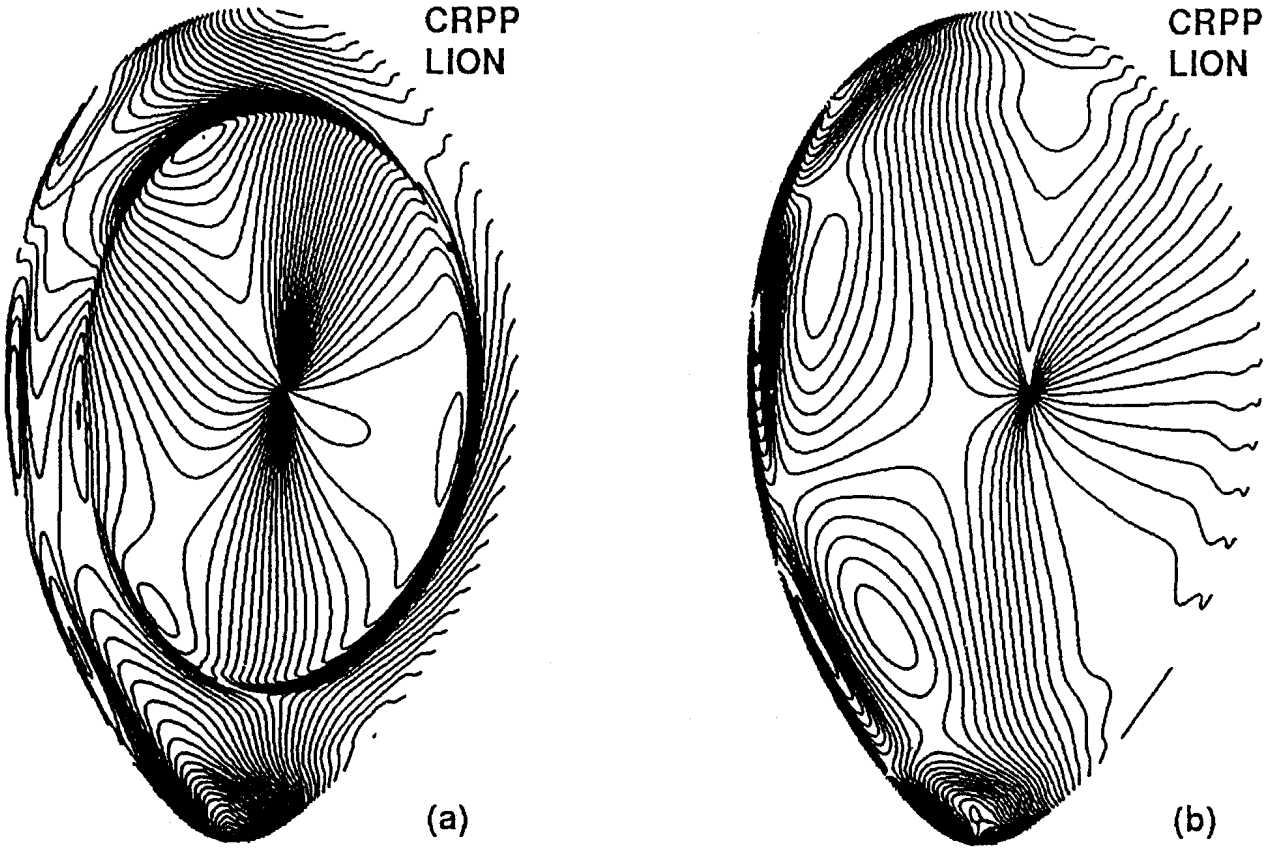

Fig.2. Contour plots of the real part of the binormal component of the wave electric field, $Re(E_b)$, of TAE modes "a" and "b" for the same parameters as in Fig.1.

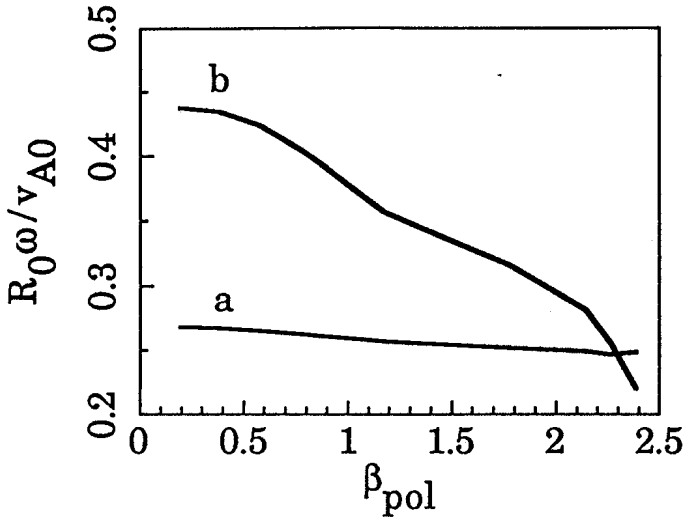

Fig.3 Eigenfrequencies of TAE modes "a" and "b" versus β_{pol} for the same parameters as in Fig.1 except the $p'(\psi)$ profile which is scaled by a constant factor.

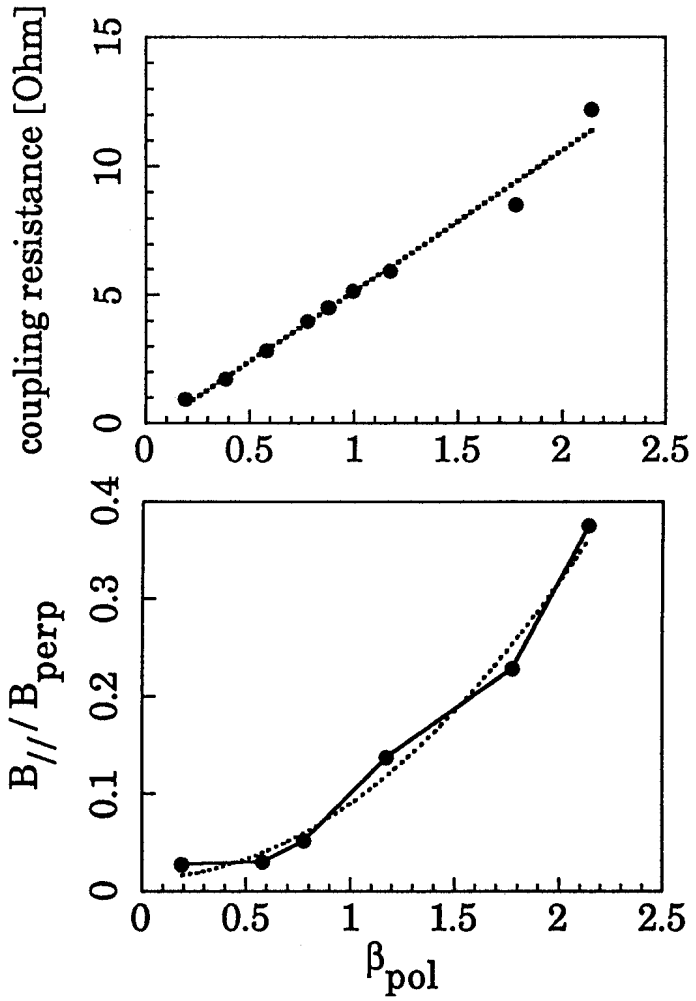

Fig.4 JET saddle coils resistive coupling (top) and compressibility (ratio of amplitudes $B_{\|}/B_{\perp}$)(bottom) of TAE mode "b" versus β_{pol} for the same parameters as in Fig.1 except the $p'(\psi)$ profile which is scaled by a constant factor.

with $(+,-,+,-)$ phasings, exciting mainly $n = 2$ modes. Saddle coils excite TAEs in the frequency range $f = 80 - 250kHz$ and EAEs (Ellipticity-Induced Alfvén Eigenmodes) in the frequency range $f = 250 - 500kHz$. The different modes can have very different couplings and this is due to different eigenmode structures. For example, the $n = 1$ mode labelled "a" in Fig.1 has an "internal" structure (Fig.2a) with a relatively modest wave amplitude at the plasma boundary and therefore a much smaller coupling than the mode labelled "b" which has the structure of an "external" mode shown in Fig.2b with a large wave amplitude throughout the plasma cross-section. We point out another basic difference between these two types of modes. The eigenfrequency of mode "a" is very close to the lower edge of the toroidicity induced gap. The mode "a" is rather insensitive to the position of the vacuum vessel whereas mode "b" is very sensitive to it: its frequency increases with a shorter plasma-wall distance and it does not exist for a wall right on the plasma boundary. The TAEs studied in Refs [1], [3], [6], [18] , being calculated with a fixed boundary, are of the "a" type ("internal").

Before we analyze the consequences of these differences in eigenmode structures on the fast particle destabilization, we point out another interesting difference in behaviour from the point of view of the strictly ideal model. Fig.3 shows the eigenfrequencies of the modes "a" and "b" for a sequence of equilibria with varying pressure. The mode "a" hardly changes its eigenfrequency and always remains just above the lower edge of the continuum gap. The fact that its frequency decreases just reflects the opening of the gap as the Shafranov shift of magnetic surfaces increases. Its coupling from the antennas remains quite small and roughly constant. Mode "b", on the other hand, is very sensitive to variations in the plasma equilibrium. Its frequency decreases strongly with increasing β_{pol}, by a factor 2 for $\beta_{pol} \simeq 2.4$. For $\beta_{pol} \simeq 2.25$ the two modes cross each other and for still higher β_{pol} mode "b" enters the Alfvén continuum. The antenna coupling of mode "b" exhibits a remarkable behaviour: it is linearily proportional to β_{pol} (see Fig.4). This is an effect of the increased Shafranov shift and a stronger variation in B_{0pol} along field lines as the equilibrium pressure is scaled up. The compressibility of the mode (finite $B_{\|}$) increases with β_{pol}(see Fig.4). The mode "b" also becomes less torsional: the ratio of amplitudes $E_n/E_\perp$ decreases from 15.4 for $\beta_{pol} = 0.78$ to 4.1 for $\beta_{pol} = 2.14$. Therefore gap modes are "Alfvén modes" only in a loosely speaking sense. One cannot a priori rule out the effect of TTMP on gap modes. This is why we chose to retain finite $B_{\|}$ in our DKE model. A practical consequence is that it will be hard to see the mode "b" for low β_{pol} values in the antenna excitation experiments. We note also that the frequency decrease with increasing beta has been seen in the DIII-D experiment [19] . The factor 2 decrease that we found is of the same order as reported in Ref. [19] . The authors of Ref. [19] have given another interpretation to this effect and named the high-beta TAE modes Beta-Induced Alfvén Eigenmodes (BAE).

3.2 Stability of TAE modes in the presence of fast ions

In what follows we analyze the $n = 1$ stability of the lowest frequency modes corresponding to modes "a" and "b" in Figs.1-4. From the point of view of the necessary condition for instability $\omega^\star > \omega$, these are the most dangerous modes. Let us first consider the mode "a" (Fig.2(a)) with the parameters $R_0 = 3m$, $n_{D0} = 5 \times 10^{19} m^{-3}$, $B_0 = 3.45T$, $T_{e0} = 10keV$, $T_{i0} = 30keV$, in the presence of fusion alpha particles. We consider fast

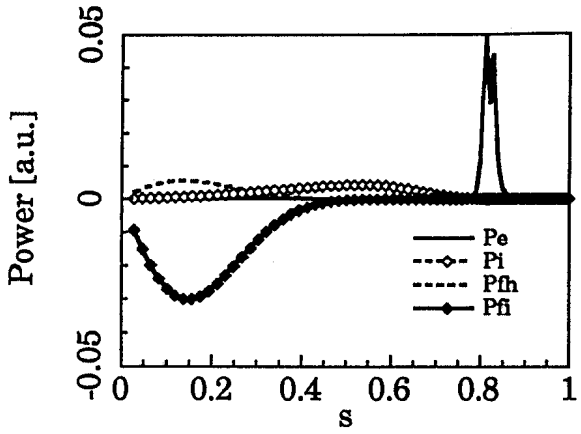

Fig.5 Radial profiles of the wave-particle DKE power transfers to electrons (continuous line), bulk ions (open symbols) and fast ions (dotted line: P_f^{homo}; filled symbols: P_f^{inhomo}) of TAE mode "a". $T_{e0} = 10keV$, $T_{i0} = 30keV$, fusion alpha particles with $n_f(s) = 10^{18}m^{-3}(1-s^2)^{22}$, $s_{1/2} = 0.176$, $v_0/v_{A0} = 1.73$. The radial variable s is $\sqrt{\psi/\psi_s}$ where ψ_s is the poloidal flux at the plasma surface. The other parameters are the same as in Fig.1.

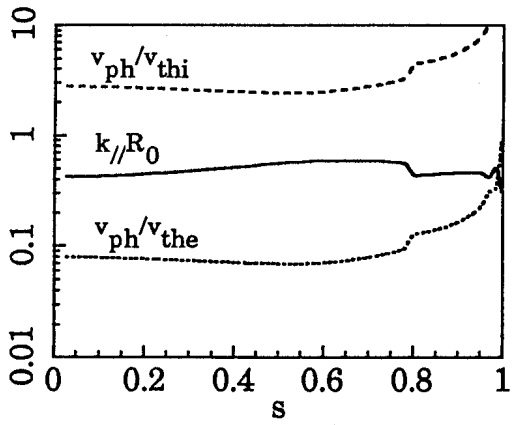

Fig.6 Radial profiles of v_p/v_{thi} (dashed line), v_p/v_{the} (dotted line) and $|k_{||}|R_0$ (continuous line) of TAE mode "a" for the same parameters as in Fig.5.

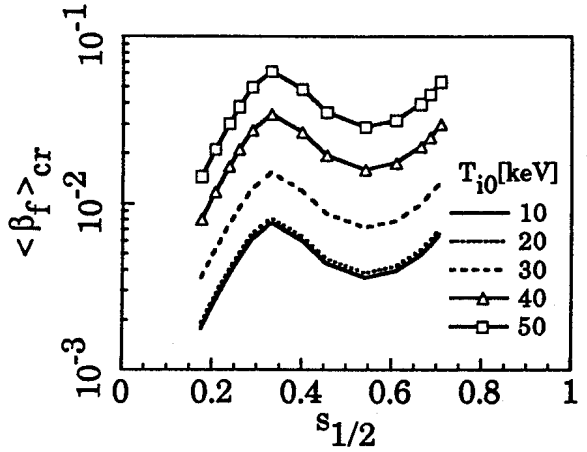

Fig.7 Volume-averaged fast particle beta for marginal stability, $< \beta_f >_{cr}$, of TAE mode "a" versus alpha particle profile half-width $s_{1/2}$, for various ion temperatures T_{i0}. The other parameters are the same as in Fig.5. (The mode is stable below the curves, unstable above).

particle density profiles defined by

$$n_f(s) = n_{f0}(1 - s^2)^{\kappa_f}, \tag{6}$$

and vary the profile peaking by varying κ_f. Moreover, we define the quantity $P(s)$ by the relation

$$P_{species} = \int_0^1 P(s)ds, \tag{7}$$

where $s = \sqrt{\psi/\psi_s}$ is the minor radius coordinate. Fig.5 shows $P(s)$ of the different species plotted versus s for $\kappa_f = 22$ which gives an alpha particle profile half-width $s_{1/2} = 0.176$. As expected the destabilizing term P_f^{inhomo} peaks around $s = 0.15$ where the alpha particle density gradient is maximal. The fast particle stabilizing term P_f^{homo} shows a similar behaviour. The electron damping, on the other hand, is localized near $s = 0.8$ ($q = 1.5$) where eigenmode gradients are very large (see Fig.2a). The ion damping is maximal near $s \simeq 0.5$. This can be understood from the factor $\exp\{-(\omega/|k_{||}|v_{thi})^2\}$ in P^{homo}. Due to the $k_{||}$ variation with respect to s, the quantity $\omega/|k_{||}|v_{thi}$ is minimal near $s \simeq 0.5$(see Fig.6). This example shows the importance of determining the overall stability globally. Local stability criteria would give instability if applied near $s = 0.2$ but stability if applied near $q = 1.5$ ($s = 0.8$). The influence of the eigenmode structure on the stability plays a crucial role. First, through the profile of eigenmode wave fields and their gradients (Fig.2). Second, through the profile of $k_{||}$ (Fig.6).

For the same parameters as in Fig.5 (except the fast particle density profile half-width $s_{1/2}$ and the central ion temperature T_{i0} which are varied) we show in Fig.7 the critical volume averaged fast-particle beta for marginal stability, $< \beta_f >_{cr}$, plotted versus the profile half-width $s_{1/2}$ for various central ion temperatures T_{i0}. The stabilizing effect of ion damping is clear for $T_{i0} \geq 20keV$. We note a remarkable behaviour of $< \beta_f >_{cr}$ vs $s_{1/2}$. For $s_{1/2} \tilde{<} 0.35$, flattening the fast particle profile is stabilizing as one can expect. But for $0.35 < s_{1/2} < 0.55$ flattening the fast particle profile actually destabilizes the mode: the reason is that an increasingly large fast particle pressure gradient is present near $s = 0.8$ ($q = 1.5$) where the eigenmode has a large amplitude (Fig.2a). This effect is not small : $< \beta_f >_{cr}$ is about a factor 2 larger for $s_{1/2} = 0.35$ than for $s_{1/2} = 0.65$. This means that about half of the fast particles would be lost if the fast particle profile widens beyond $s_{1/2} = 0.35$. For $s_{1/2} > 0.65$, flattening the fast particle profile is again stabilizing because of the reduced fast particle pressure gradient.

3.3 Dependence on the fast particle profile width $s_{1/2}$, bulk plasma β, v_0/v_{A0} and ω/ω_{ci}

In this section we consider the same sequence of plasma MHD equilibria as before but consider the case where both bulk ions and fast ions are deuterium species. Fast ions birth energy is $75keV$. The temperature and density profiles are chosen as $T_e(s) = T_{e0}(1 - s^2)^{1/2}$, $T_i(s) = T_{i0}(1 - s^2)^{1/2}$, $n(s) = n_0(1 - 0.9s^2)^{1/2}$ and $n_f(s) = n_{f0}(1 - s^2)^{\kappa_f}$. We keep the ratio T_i/T_e constant at 1.25. Different values of bulk β, v_0/v_{A0} and ω/ω_{ci} are obtained by varying the bulk density n_0, temperatures T_{i0} and T_{e0} and magnetic field B_0 each over a wide range of values:

$$B_0 \;=\; 0.6 - 2.25 \quad T$$

$$
\begin{aligned}
n_0 &= 1.3 - 30 \times 10^{19} \quad m^{-3} \\
T_{i0} &= 0.15 - 12.8 \quad keV \\
T_{e0} &= 0.12 - 10.3 \quad keV
\end{aligned}
$$

We set the major radius of magnetic axis at $1.8m$. These parameters overlap those of DIII-D TAE excitation experiments with NB injection [8] [9] [19] . We study the fast particle critical beta corresponding to marginal stability of TAE modes "a" and "b" for a range of fast particle profile widths $s_{1/2}$ obtained by varying the coefficient κ_f.

The damping on bulk species depends on the ratios $\omega/|k_{||}|v_{the}$, $\omega/|k_{||}|v_{thi}$ and ω/ω_{ci}. The TAE eigenfrequencies ω scale proportionally to the Alfvén velocity on axis v_{A0}, so the ratio $\omega/|k_{||}|v_{the}$ is proportional to $1/\beta_e$,$\omega/|k_{||}|v_{thi}$ is proportional to $1/\beta_i$, and $(\omega/\omega_{ci})^2$ is proportional to $1/n_0$. Thus for given $T_e(s)$, $T_i(s)$, $n(s)$ profile shapes and for a fixed T_{i0}/T_{e0} ratio the damping on bulk ions and electrons of a given TAE depends only on the plasma beta and on the bulk density n_0. The DKE power on fast ions depends on the ratio v_p/v_0 and on the profile width $s_{1/2}$ through the parameter κ_f in Eq.(6). For a given TAE mode, v_p scales proportionally to v_{A0}. So the overall global stability properties of a given TAE mode in a plasma with given profile shapes of $T_i(s)$, $T_e(s)$ and $n_i(s)$ and a fixed T_{i0}/T_{e0} ratio are determined by the plasma beta, the ratio ω/ω_{ci} (bulk density n_0), the fast particle profile width $s_{1/2}$ and the ratio v_0/v_{A0}. The global stability of TAEs depends also on the eigenmode wavefield structure as was illustrated in the previous section.

Before studying the stability of TAE modes in the presence of fast particles, we have analyzed the DKE powers on electrons and bulk ions. For a given TAE mode and a fixed plasma beta, we found that P_e depends linearly on $(\omega/\omega_{ci})^2$, for any combination of T_{e0}, n_{e0} and B_0 giving the same beta. So P_e depends on β_e and n_0. On the other hand we have found that P_i depends very weakly on ω/ω_{ci} and can be considered as a function of β_i only.

We show in Fig.8 the critical volume-averaged fast particle beta, $< \beta_f >_{cr}$, plotted as a function of the fast particle profile half-width $s_{1/2}$, for various ratios of the birth velocity to the Alfvén velocity on axis, v_0/v_{A0}. All data in Fig.8 has been calculated with the same equilibrium plasma beta of 3% and for the "internal" $n = 1$ TAE mode ("a" in Figs 1-3). The ratio v_0/v_{A0} was varied by changing the density n_0 and the temperature T_{i0}, T_{e0} as $1/n_0$, keeping B_0 constant, so that β is constant. As in Fig.7, we have a remarkable behaviour of $< \beta_f >_{cr}$ vs $s_{1/2}$. For $s \tilde{<} 0.35$ widening the fast particle profile is stabilizing because the fast particle pressure gradient is decreased. But for $s \tilde{>} 0.35$ the opposite is true: although the fast particle pressure gradient term is decreasing, the destabilization comes from the increasingly large fast ion pressure gradient near the $q = 1.5$ surface where the TAE wave field and its gradient are large (see Fig.2a). For $s_{1/2}$ near 0.6 the two effects balance about each other and for still larger $s_{1/2}$ values the stabilizing effect of flattening the fast particle profile dominates.

We note that for $v_0/v_{A0} \tilde{>} 1$ the $< \beta_f >_{cr}$ is lower for $s_{1/2} = 0.7$ (which corresponds to $n_f(s) = n_{f0}(1 - s^2)$) than for $s_{1/2} = 0.35$ (which corresponds to $n_f(s) = n_{f0}(1 - s^2)^6$). This particular behaviour is a consequence of the TAE mode structure. By no means could a local theory predict such a behaviour. It may have implications on the evolution of the fast particle contents in the discharge: if this mode is close to marginal stability and if $s_{1/2}$ goes beyond 0.35, the loss of fast particles, flattening the profile, would make the mode more unstable, so that fast particles would continue to be expelled until $s_{1/2}$ is

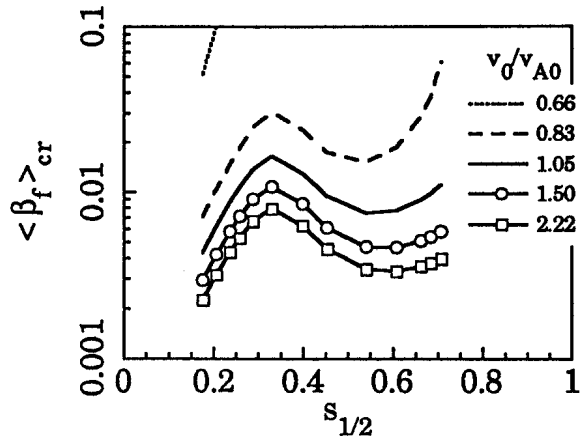

Fig.8 Volume-averaged fast particle beta for marginal stability, $< \beta_f >_{cr}$, of TAE mode "a" versus fast ion density profile half-width $s_{1/2}$, for various values of v_0/v_{A0} and fixed plasma bulk beta of 3% and $T_{i0} = 1.25T_{e0}$. v_0/v_{A0} is changed by varying the bulk density n_0 and the temperatures T_{i0} and T_{e0} as $1/n_0$, keeping B_0 constant. $R_0 = 1.8m$, $B_0 = 0.74T$, deuterium fast particles injected at $75keV$.

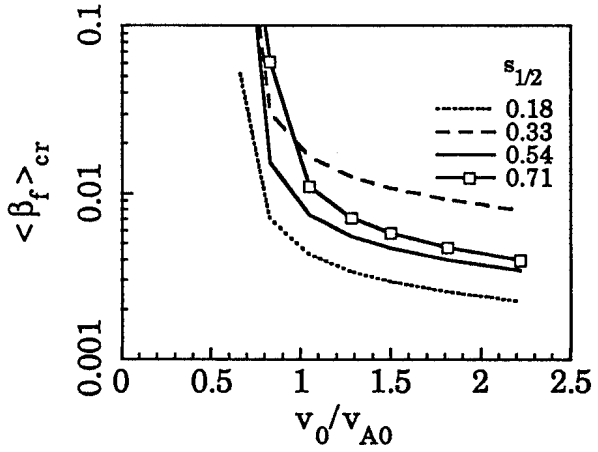

Fig.9 $< \beta_f >_{cr}$ of TAE mode "a" versus v_0/v_{A0} for various values of fast ion density profile half-width $s_{1/2}$ for $\beta = 3\%$. Other parameters: same as Fig.8.

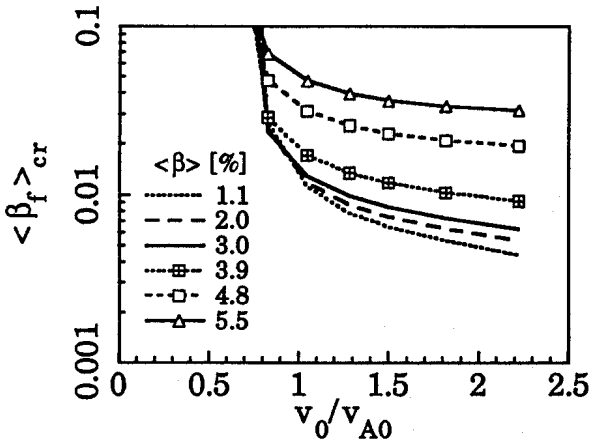

Fig.10 $< \beta_f >_{cr}$ of TAE mode "a" versus v_0/v_{A0} for various values of plasma bulk β for a fixed fast ion density profile half-width $s_{1/2} = 0.4$. Other parameters: same as Fig.8.

about 0.6. Only then can the fast particle profile build up again in the center. But in the meantime, we see from Fig.8 that about half of the energy content of fast particles would have been lost. Note that this may be related to the "bursts" of expelled fast particles sometimes seen in the experiments [7]-[9] . Of course a nonlinear study is needed to properly predict the time behaviour of fast particles [20] .

For the same parameters as in Fig.8, we show in Fig.9 the behaviour of $< \beta_f >_{cr}$ versus the ratio v_0/v_{A0} for different fast particle density profile widths $s_{1/2}$. For a given $s_{1/2}$, $< \beta_f >_{cr}$ is a monotonically decreasing function of v_0/v_{A0}. We note that this TAE mode can become unstable even for values of v_0/v_{A0} as small as about 0.6. This is due to the behaviour of $|k_{\|}|$ of the mode, which is not exactly ω/v_A, but is lower in this case due to the presence of "sidebands" in the poloidal Fourier mode numbers m: the poloidal Fourier decomposition of the eigenmode wavefield shows actually a rather broad m spectrum, due to the small aspect ratio, the elongation and shape of this configuration.

For a given fast ion profile width $s_{1/2} = 0.4$ and plasmas of different beta values we show in Fig.10 the $< \beta_f >_{cr}$ versus v_0/v_{A0}, for the same parameters as in Fig.9 except the plasma beta. For all β values $< \beta_f >_{cr}$ is a decreasing function of v_0/v_{A0}. For v_0/v_{A0} close to 0.7, little effect of beta on $< \beta_f >_{cr}$ is seen: in this region of parameter space, the stability is determined mainly by the competition between P_f^{inhomo} and P_f^{homo} , and the stability diagram corresponds in fact to a threshhold in v_0/v_{A0} of about 0.7. For larger values of v_0/v_{A0}, increasing beta is always stabilizing through enhanced electron and ion Landau dampings. We note that for $v_0/v_{A0} < 2$ and $\beta = 1\%$ we have $< \beta_f >_{cr} > 0.4\%$, which is indeed larger than the estimated $< \beta_\alpha >$ in TFTR D-T experiments [21] in which no sign of TAE activity was reported.

In the next three figures (11,12 and 13) we show the corresponding results of Figs 8,9,10 but for the $n = 1$ "external" mode ("b"). In Fig.11 the values of $< \beta_f >_{cr}$ are plotted versus the fast profile width $s_{1/2}$, for a given bulk beta of 3% and for various values of v_0/v_{A0} obtained by varying n_{i0} and T_{e0}, T_{i0} as $1/n_0$. For $s_{1/2} < 0.4$, $< \beta_f >_{cr}$ is increasing with $s_{1/2}$ as the fast ion gradient decreases. For $s_{1/2} \tilde{>} 0.4$ the behaviour of $< \beta_f >_{cr}$ versus $s_{1/2}$ depends dramatically on the value of v_0/v_{A0}. For $v_0/v_{A0} \tilde{<} 1.5$, $< \beta_f >_{cr}$ monotonically increases with $s_{1/2}$. But for $v_0/v_{A0} \tilde{>} 1.5$ the opposite is true. This particular behaviour, which is quite different from that of the "internal" $n = 1$ mode (Fig.8), must be related to the global eigenmode wavefield structure, which is rather flat in the center but has maximum amplitude in the outer region(Fig.2b). For v_0/v_{A0} above 1.5, the ratio v_0/v_p in the outer region is above unity for this mode: fast particles, if present there, will be destabilizing. This is the reason for the decrease in $< \beta_f >_{cr}$ versus $s_{1/2}$ for $s_{1/2} \tilde{>} 0.4$. For v_0/v_{A0} below 1.5 the ratio v_0/v_p is below unity in the outer region where the mode amplitude is large and therefore no destabilization occurs by flattening the fast particle profile.

In Fig.12 $< \beta_f >_{cr}$ is represented versus v_0/v_{A0} for various profile widths $s_{1/2}$. For this bulk beta value of 3%, $< \beta_f >_{cr}$ is decreasing with v_0/v_{A0} in all cases. We note that this mode can be destabilized for values of v_0/v_{A0} as low as about 0.8.

The behaviour of $< \beta_f >_{cr}$ versus v_0/v_{A0} for this "external" $n = 1$ mode has a remarkable dependence on plasma beta, which is shown in Fig.13. For large v_0/v_{A0} the TAE is stabilized when beta increases, due to enhanced electron and ion Landau damping. On the other hand, increasing beta is destabilizing for small v_0/v_{A0}: the minimum v_0/v_{A0} for instability goes from 1 for $\beta = 1\%$ down to 0.7 for $\beta = 5.5\%$. Increasing beta is lowering

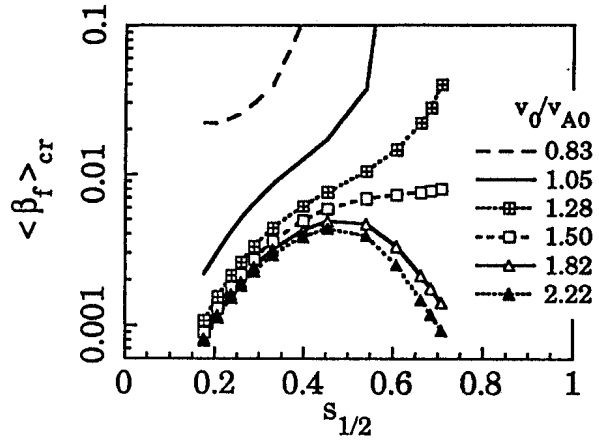

Fig.11 $< \beta_f >_{cr}$ of TAE mode "b" versus fast ion density profile half-width $s_{1/2}$ for various values of v_0/v_{A0} and fixed plasma bulk beta of 3%. Other parameters: same as Fig.8.

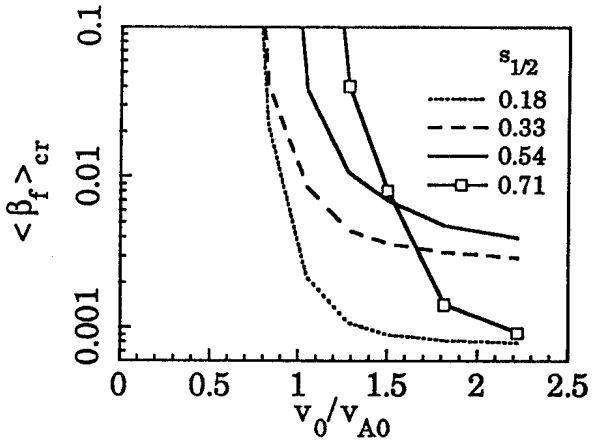

Fig.12 $< \beta_f >_{cr}$ of TAE mode "b" versus v_0/v_{A0} for various values of $s_{1/2}$. Other parameters: same as Fig.8.

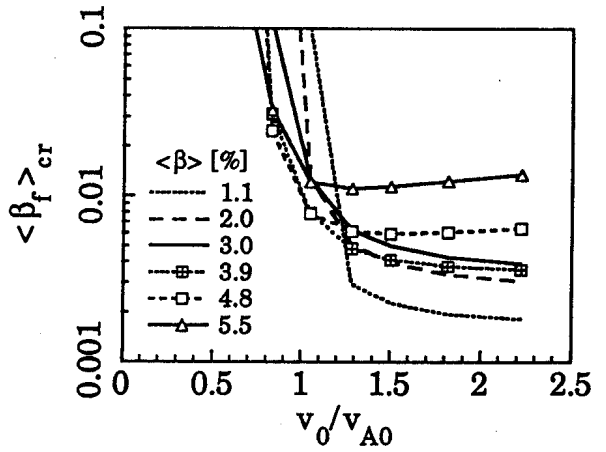

Fig.13 $< \beta_f >_{cr}$ of TAE mode "b" versus v_0/v_{A0} for various values of plasma bulk β for a fixed fast ion density profile half-width $s_{1/2} = 0.4$. Other parameters: same as Fig.8.

the eigenfrequency of this mode (see Fig.3). Consequently the parallel phase velocity is decreasing and more fast particles can destabilize the mode. Therefore the threshhold in v_0/v_{A0} is going down with increasing beta for this mode. This is not the case for mode "a" (see Fig.10) because it is rather insensitive to beta (see Fig.3).

4 Discussion

Our model is based on a certain number of assumptions and simplifications that we can summarize as follows. First, the kinetic effects have been considered as a small perturbation of the ideal TAE wave fields. The dissipative contributions of the kinetic effects have been taken into account (damping and drive) but not their effect on dispersion. Since those cannot be considered small in the vicinity of Alfvén resonant surfaces, we have restricted our analysis to cases where TAEs have no Alfvén resonances and thus no continuum damping (in other words, no conversion to KAW or SQEW). In this sense our results can be considered as a pessimistic evaluation of the TAE stability especially for low n modes for which continuum damping is most efficient, since it goes as $n^{-3/2}$ for high n [16],[17] . Second, we have neglected trapped particle and finite drift orbit width effects.

On the other hand, we have solved the problem globally in exact toroidal geometry and we have shown that this approach can give very different results from those of local models (see e.g.Fig.5). The global eigenmode wavefield structure is an important factor determining the instability threshhold. In particular, $< \beta_f >_{cr}$ can be a non-monotonic function of the fast particle density profile width and in many cases flattening the fast particle density profile is destabilizing (Figs 8 and 10). This may have consequences on the existence of bursts of expelled fast particles that are seen in some experiments [7]-[9]

.

We have identified and studied two types of TAEs: type "a" (internal) and type "b" (external) having different wave fields (Fig.2) and therefore different stability properties (Fig.8-13). They behave differently with respect to equilibrium plasma parameters, in particular the plasma β. They also couple differently to an antenna (Fig.1): type "a" TAEs couple rather weakly and independently of β, wheras type "b" TAEs couple better and approximately proportionally to β due to the increased compressibility of the mode (Fig.4).

Finite β affects the TAEs and their stability in the following way. Increasing β is always stabilizing type "a" TAEs in strengthening the damping on bulk species (Fig.10). The effects on type "b" TAEs are more complex. The real part of the eigenfrequency decreases with β (Fig.3). This was seen in the DIII-D experiment [19] and already computed for circular cross-sections [11] . Therefore the parallel phase velocity decreases and more fast particles can resonantly interact with the wave and destabilize it. This destabilizing effect competes with the increased damping on bulk species with increasing β and the final result can be summarized as a decrease in the v_0/v_A instability threshhold ($v_0/v_A < 1$) and an increase in $< \beta_f >_{cr}$ for v_0/v_{A0} above unity (Fig.13). We note that the v_0/v_{A0} instability threshhold below unity (~ 0.7) is in a good agreement with DIII-D experiment [9] .

The parameters determining the TAE stability are: v_0/v_{A0}, β and n_0, for the damping on bulk species and, in addition, β_f and $s_{1/2}$ for the drive and damping on fast ions. Although the computations presented in this paper were not made with the intent to

analyze a particular experimental shot, we can give some clues as to how our results should be interpreted so that a comparison with experiment can be made. The time evolution of a discharge should be analyzed as a motion in the 5-dimensional parameter space v_0/v_{A0}, β, n_0, β_f, $s_{1/2}$ (note that additional parameters such as plasma shape, current, density and temperature profiles could also be important but were not varied in this paper). The instability threshholds calculated with our model can be viewed as $< \beta_f >_{cr}$ surfaces function of the four other parameters. Instability occurs when the trajectory of the discharge crosses a $< \beta_f >_{cr}$ surface. Let us consider the example of NB injection and, for the sake of simplicity, let us assume that $s_{1/2}$ is constant. As NBI is switched on, there is a β_f increase, a bulk β increase and quite frequently a density increase, which implies an increase in v_0/v_{A0} if B_0 is kept constant. Let us consider the stability of type "b" TAE (Fig.13). The trajectory of the shot projected on Fig.13 is then a line going in the upward right side direction. But β is increasing, which means that if v_0/v_{A0} is of order unity or even lower and β_f of the order of 1%, the instability threshhold will be crossed for any value of β.We note that these values of β_f and v_0/v_{A0} are in close agreement with the DIII-D experiments (see Fig.10 of Ref. [9]). There may be other shots that evolve in such a way that the bulk β increases fast enough so that the shot trajectory remains below $< \beta_f >_{cr}$ at any time; this can happen even if v_0/v_{A0} is much larger than 1. Although this is also in qualitative agreement with experiment [9] , a more careful comparison should be made, including the study of higher n modes.

5 Conclusions

We have developed a hybrid fluid kinetic model for the quantitative prediction of the global linear stability of low n TAEs in the presence of a fast ion population. We have applied this model to a wide variety of cases in order to study the dependence of the TAE stability on a certain number of parameters which were varied over a wide range. The critical volume-averaged fast ion beta corresponding to marginal stability, $< \beta_f >_{cr}$, was studied versus the four parameters: v_0/v_{A0}, β, n_0 and $s_{1/2}$. Typical values of $< \beta_f >_{cr}$ are, for v_0/v_{A0} near unity, of the order of 1%, which is in rather good overall agreement with the DIII-D experiment [9] . Only for extremely peaked fast ion density profiles ($s_{1/2} \tilde{<} 0.2$) can $< \beta_f >_{cr}$ become of the order of 0.1%. The finite β effects on type "b" (external) TAEs are a strong decrease in real eigenfrequency, a decrease in the v_0/v_{A0} threshhold and a stabilizing effect for v_0/v_{A0} above unity. All of these is in agreement with experiments so far. More work is necessary to further assess the validity and applicability of our model, in particular a more detailed case-by-case analysis of some experiments. The saddle coil experiment at JET will also provide interesting material for a comparison with theory. In the future, the stability of higher n modes will be analyzed and our model will be applied to predict instability threshholds in reactor tokamak plasmas (ITER).

Acknowledgments
This work was partly supported by the Swiss National Science Foundation.

References

[1] CHENG, C.Z., CHANCE, M.S., Phys.Fluids **29** (1986) 3695.

[2] FU, G.Y., VAN DAM, J.W., Phys.Fluids B **1** (1989) 1949.

[3] CHENG, C.Z., Phys.Fluids B **3** (1991) 2463.

[4] BELIKOV, V.S., KOLESNICHENKO, YA.I., SILIVRA, D.A., Nucl.Fusion **32** (1992) 1399.

[5] BIGLARI, H., ZONCA, F., CHEN, L., Phys.Fluids B **4** (1992) 2385.

[6] FU, G.Y., CHENG, C.Z., WONG, K.L., Phys.Fluids B **5** (1993) 4040.

[7] WONG, K.L., FONCK, R.J., PAUL, S.F., ET AL., Phys.Rev.Lett. **66** (1991) 1874.

[8] HEIDBRINK, W.W., STRAIT, E.J., DOYLE, E., ET AL., Nucl.Fusion **31** (1991) 1635.

[9] STRAIT, E.J., HEIDBRINK, W.W., TURNBULL, A.D., CHU, M.S., DUONG, H.H., Nucl.Fusion **33** (1993) 1849.

[10] METT, R.R., MAHAJAN, S.M., Phys.Fluids B **4** (1992) 2885.

[11] VILLARD, L., FU, G.Y., Nucl.Fusion **32** (1992) 1695.

[12] LUTJENS, H., BONDESON, A., ROY, A., Comput.Phys.Commun. **69** (1992) 287.

[13] BRUNNER, S., VILLARD, L., VACLAVIK, J., A Kinetic Model for the Global Power Transfer between Particles and MHD Waves, in these proceedings.

[14] VILLARD, L., APPERT, K., GRUBER, R., VACLAVIK, J., Comput.Phys.Rep. **4** (1986) 95.

[15] APPERT, K., HELLSTEN, T., LUTJENS, H., SAUTER, O., VACLAVIK, J., VILLARD, L., in Plasma Physics (Proc. 7th Int.Conf.Kiev, 1987), Invited papers, Vol.2, World Scientific, Singapore (1987) 1230.

[16] ROSENBLUTH, M.N., BERK, H.L., VAN DAM, J.W., LINDBERG, D.M., Phys.Rev.Lett. **68** (1992) 596.

[17] ZONCA, F., CHEN, L., Phys.Rev.Lett. **68** (1992) 592.

[18] POEDTS, S., KERNER, W., GOEDBLOED, J.P., KEEGAN, B., HUYSMANS, G.T.A., SHWARTZ, E., Plasma Phys.Control.Fusion **34** (1992) 1397.

[19] HEIDBRINK, W.W., STRAIT, E.J., CHU, M.S., TURNBULL, A.D., Phys.Rev.Lett. **71** (1993) 855.

[20] BERK, H.L., BREIZMAN, B.N., YE, H., Phys.Rev.Lett. **68** (1992) 3563.

[21] STRACHAN, J.D., ADLER, H., ALLING, P., ET AL., Phys.Rev.Lett. **72** (1994) 3526.

NONLINEAR INTERACTION OF LOWER HYBRID WAVES

C. Bruderer, J. Vaclavik and K. Appert

Centre de Recherches en Physique des Plasmas,
Association Euratom–Confédération Suisse,
Ecole Polytechnique Fédérale de Lausanne,
21, av. des Bains, 1007 Lausanne, Switzerland

1 Introduction

Lower hybrid current drive has proved very successful in a number of experiments [1, 2, 3]. Power absorption occurs through electron Landau damping; lower hybrid waves are therefore well suited for current profile control. The wave spectrum extends from the minimum $k_{||}$ needed for accessibility up to a maximum value above which strong absorption at the plasma edge occurs [4]. This spectrum corresponds to a range of resonant parallel velocities extending from a few times thermal up to relativistic velocities. There is still no satisfactory explanation on how a consistent population of suprathermal electron is generated with a launched spectrum corresponding to velocities well above the bulk of the distribution function [5].

S. Succi et al. [6] had shown that plasma current was extremely sensitive to the presence of a small, high-$N_{||}$ component in the r.f. power source spectral distribution. In this paper, we show that a model including nonlinear interactions is able to produce an upshift in the parallel refraction index sufficient to drive significative currents.

2 Model

Electrostatic perturbations are considered, in a cold, homogeneous plasma in slab geometry. The basic equations are the fluid and Poisson's equations in reciprocal (Fourier) k-space. Ions are assumed to be unmagnetized as $\omega_{ci} << \omega << \omega_{ce}$.

2.1 Nonlinear part

The nonlinear part of the equations has terms in $\vec{k_\perp} \times \vec{k'_\perp}$ that are very large; a 3 dimensional description is therefore necessary. As there is only one anisotropic direction, the problem can be reduced to 2 variables, u and v, given by the following relations:

$$\left.\begin{aligned} u &= \alpha x + \beta z \\ v &= \alpha y + \beta z \end{aligned}\right\} \qquad (1)$$

with $\alpha^2 + \beta^2 = 1$ and $\beta^2 = sin^2\theta/(1 + sin(2\phi)\ cos^2\theta)$, where z is the direction of the magnetic axis, θ and ϕ are given in Fig.1. The new wave vectors satisfy:

$$\left.\begin{aligned} k_x &= \alpha K_u \\ k_y &= \alpha K_v \\ k_{||} &= \beta(K_u + K_v) \end{aligned}\right\} \qquad (2)$$

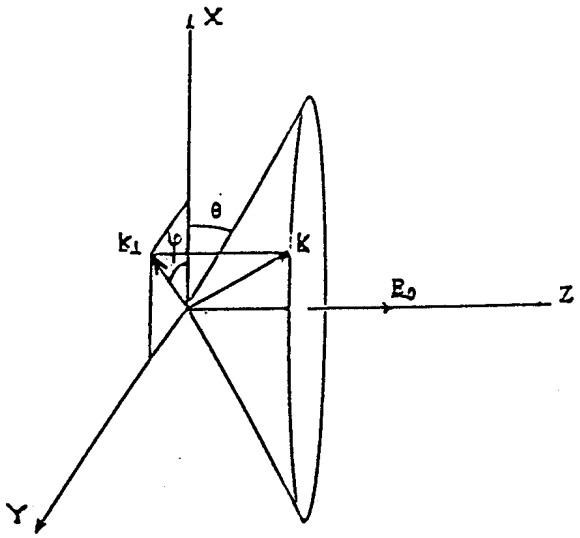

Fig.1
Wave vectors of modes with same frequencies generate a cone in (x,y,z) space

Formally,the nonlinear problem can be reduced to the following system:

$$\partial_t \vec{\psi} + \vec{\vec{M}}\,\vec{\psi} = \vec{R} \quad where \quad \vec{\psi} = \begin{pmatrix} n_e \\ \vec{v_e} \\ n_i \\ \vec{v_i} \end{pmatrix} \tag{3}$$

$\vec{R}$ representing the quadratic nonlinear terms.

The solution considering both polarizations of the lower-hybrid branch reads:

$$\vec{\psi}\left(\vec{K},t\right) = \sum_{n=1}^{2} c_n\left(\vec{K},t\right)\vec{\phi}_n\left(\vec{K}\right)e^{-i\omega_n(\vec{K})t} \tag{4}$$

where $\vec{\phi}_n$ are the linear orthonormal eigenvectors and the frequencies satisfy the dispersion relation:

$$\omega^2 = \frac{\omega_{pi}^2 + \omega_{pe}^2 sin^2\theta}{1 + \left(\frac{\omega_p}{\omega_{ce}}\right)^2} \tag{5}$$

The nonlinear evolution of the coefficients $c_n\left(\vec{K},t\right)$ is given by:

$$\left[\partial_t c_n\left(\vec{K},t\right)\right]_{NL} = \vec{\phi}_n^{\dagger}\left(\vec{K}\right)\vec{R}\,e^{i\omega_n(\vec{K})t} \tag{6}$$

2.2 Quasilinear Part

Electron Landau damping is taken into account quasilinearly. Since electrons are accelerated in the parallel direction, the distribution function is considered in a one dimensional approximation. Its evolution is governed by:

$$\partial_t f = (2+Z)\,\nu_0\partial_v\left[\frac{1}{v^3}\left(vf + \partial_v f\right)\right] + \partial_v D_{lh}\partial_v f \tag{7}$$

In Eq.(7), the first term on the right-hand side is the 1D Fokker-Planck operator including electron-electron and electron-ion collisionnal effects, without pitch-angle scattering. Z

denotes the charge state and $\nu_0 = (log\Lambda\omega_{pe}^3)/(4\pi n_0 v_{the}^3)$. The second term is the quasilinear diffusion term :

$$D_{lh}(v) = \pi \int \frac{dK_u dK_v}{(2\pi)^2} \left(\frac{k_\parallel}{|\vec{k}|}\right)^2 \delta\left(\omega_{\vec{K}} - k_\parallel v\right) W\left(\vec{K}\right) \tag{8}$$

$\int W\left(\vec{K}\right) dK_u dK_v$ representing the linear wave energy density.

Taking ion viscosity into account, the quasilinear evolution of the coefficients $c_n\left(\vec{K}\right)$ reads:

$$\left[\partial_t c_n\left(\vec{K},t\right)\right]_{QL} = \left(\Gamma\left(\vec{K},t\right) - \frac{\nu_0 Z}{4} - \eta k^2\right) c_n\left(\vec{K},t\right) + \frac{S\left(\vec{K}\right)}{2c_n^*\left(\vec{K},t\right)} \tag{9}$$

where $\Gamma = \frac{\pi}{2}\omega sign\left(k_\parallel\right)\left(\frac{1}{|\vec{k}|}\right)^2 \partial_v f|_{v=\omega/k_\parallel}$ is the electron Landau damping term, η the viscosity coefficient and S an external source which drives the waves. All quantities throughout Eq.(7) to Eq.(9) are normalized according to $k \rightarrow k/\lambda_D, t \rightarrow t/\omega_{pe}, v \rightarrow v v_{the}, f \rightarrow f n_0/v_{the}^3, W \rightarrow W 4\pi n_0 T_e \lambda_D^3$.

Symbolically, the waves evolve as :

$$\partial_t c_n\left(\vec{K},t\right) = \left[\partial_t c_n\left(\vec{K},t\right)\right]_{NL} + \left[\partial_t c_n\left(\vec{K},t\right)\right]_{QL} \tag{10}$$

3 Results

A single charged deuterium plasma at low density ($n_e = 7 \times 10^{18} m^{-3}$) in a toroidal field of 3 T, with cold ions and electrons at a temperature of 1 keV is considered. The frequency range of the numerically representable spectrum extends from $\omega_{LH} = 2.37 \times 10^9$ rad/s to 2 ω_{LH}. In order to reach steady state in reasonable computational times, the collision term in (9) has been chosen to be $10\nu_0/4$ (0.97×10^6 rad/s). The viscosity term has been chosen so that its value at thermal velocity is comparable with the collision term. Initially, the linear wave energy represents 6% of the electron thermal energy, and corresponds to a maximal local perturbation in density of 37 % for the ions and 3 % for the electrons. 99.95% of the

initial energy is put into modes with velocities higher than 10 v_{the} (See Fig.2). 80% (resp.

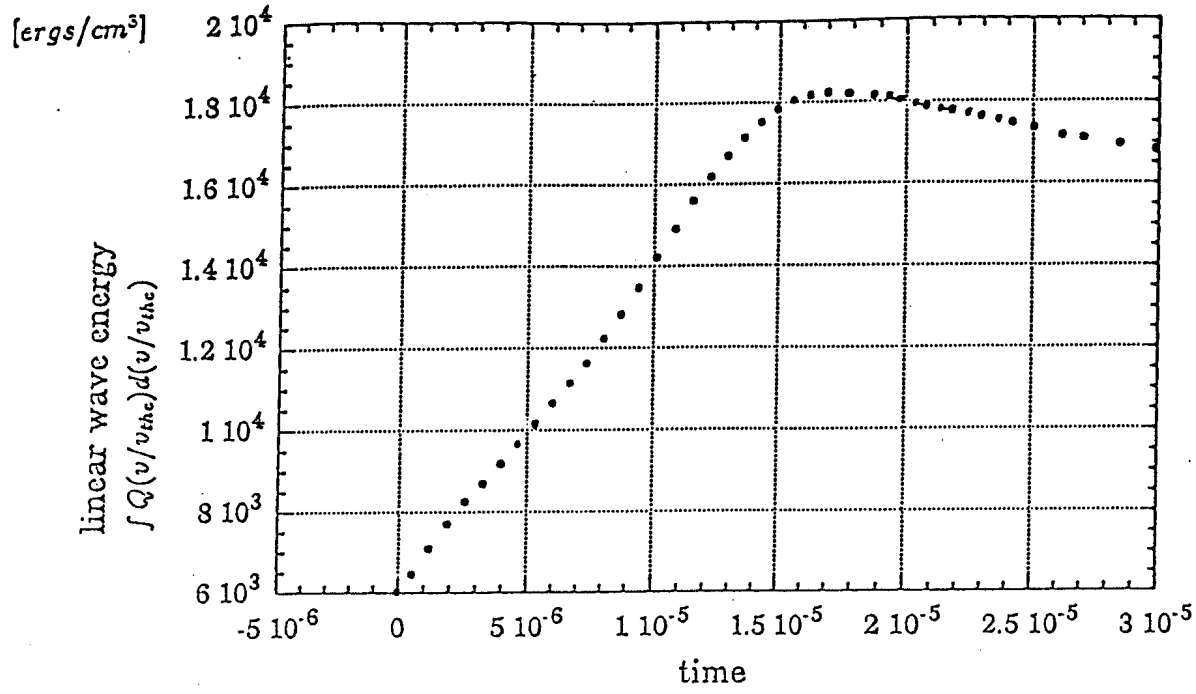

Fig. 3 *Linear Wave Energy Density vs time*

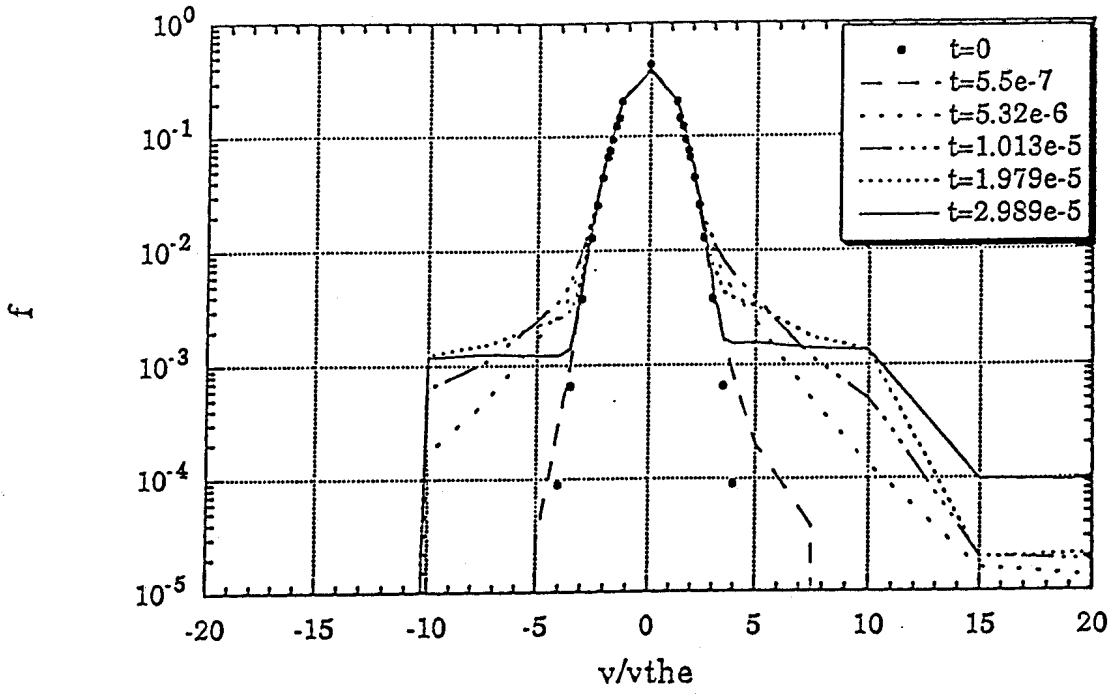

Fig. 4 *Electron distribution function at different times*

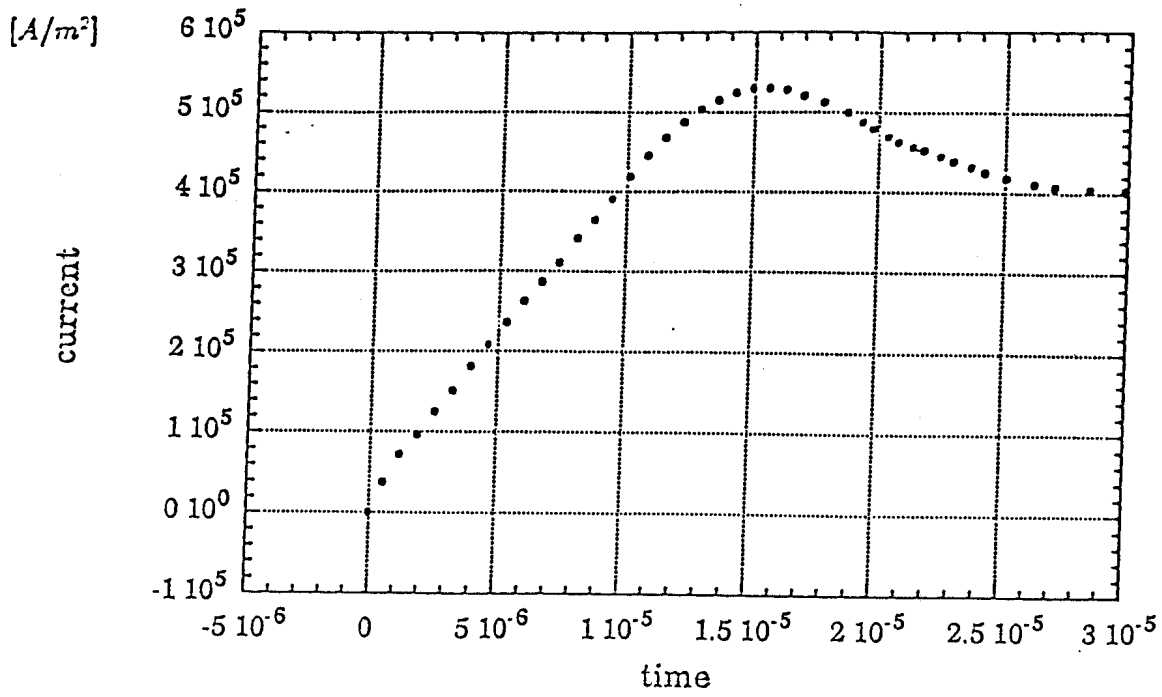

Fig. 5 *Current density vs time*

4 Conclusion

A 3D nonlinear wave code including quasilinear evolution of the electron distribution function has been developed. We have shown that nonlinear interactions are able to fill in the spectral gap.

In the results shown, the power input is very high, because the collision frequency has been arbitrarily raised in order to run the case in reasonable computational times. A faster converging time evolution numerical scheme has to be implemented.

5 Acknowledgment

This work was supported in part by the Swiss National Science Foundation.

References

[1] S. Bernabei et al., "Lower-Hybrid Current Drive in the PLT Tokamak", *Phys. Rev. Letters*, vol. 49, No 17, p. 1255, 1982

[2] JT60 Team, *Plasma Phys. Control. Fusion*, vol. 32, p. 853, 1990

[3] JET team, "Non inductive current drive in Jet", *IAEA-CN-561E-1-1*,1992

[4] T. Stix,"The theory of plasma waves", p.62

[5] Reviews of Plasma Physics, vol. 17 (1992), ed. by B.B. Kadomtsev

[6] S. Succi, K. Appert, J. Vaclavik, "Generation of suprathermal electrons interacting with waves in lower-hybrid range of frequency revisited", *Plasma Physics and Controlled Fusion*, vol. 27, No 8, p. 863, 1985

A Kinetic Model for the Global Power Transfer between Particles and MHD Waves.

S.Brunner, L.Villard and J. Vaclavik

Centre de Recherches en Physique des Plasmas

Association Euratom - Confédération Suisse

Ecole Polytechnique Fédérale de Lausanne

21, av. des Bains – CH-1007 Lausanne/Switzerland

We present here the calculations that lead to the power absorption formulas used in the companion paper [1] in the study of possible destabilization of Alfvén modes by high-energy ions.

We consider a hot plasma in axisymmetric equilibria $\vec{B}_0 = T\nabla\varphi + \nabla\varphi \times \nabla\psi$ where T is the toroidal flux function, φ is the toroidal angle and ψ the poloidal flux function. The plasma is perturbed by EM fields $(\vec{E}, \vec{B})$. The evolution equation used for the plasma species is the Drift Kinetic Equation (DKE)

$$\frac{Df}{Dt} = \left[\frac{\partial}{\partial t} + \vec{v_g} \cdot \frac{\partial}{\partial \vec{X}} + \frac{d\epsilon}{dt}\frac{\partial}{\partial \epsilon} + \frac{d\mu}{dt}\frac{\partial}{\partial \mu}\right] f(\vec{X}, \epsilon, \mu, t) = 0, \tag{1}$$

where $\vec{X}$ is the guiding center, $\epsilon = \frac{1}{2}(v_{\|}^2 + v_{\perp}^2)$, $\mu = v_{\perp}^2/2B_0$, $\vec{v_g} = v_{\|}\ \vec{e}_B + \vec{v_E} + \vec{v_d}$, $\vec{v_E} = \vec{E} \times (\vec{B}_0 + \vec{B})/B^2$, $\vec{v_d} = (m/qB)\ \vec{e}_B \times \left(v_{\perp}^2/2 + v_{\|}^2\right) \nabla \ln B$, $B = \mid \vec{B}_0 + \vec{B} \mid$ the total magnetic field and $\vec{e}_B = (\vec{B}_0 + \vec{B})/B$. Furthermore we define the unit vectors: $\vec{e}_{\|} = \vec{B}_0 / \mid \vec{B}_0 \mid$, $\vec{e}_n = \nabla\psi/|\nabla\psi|$, $\vec{e}_p = (\nabla\varphi \times \nabla\psi)/|\nabla\varphi \times \nabla\psi|$ and $\vec{e}_b = \vec{e}_{\|} \times \vec{e}_n$.

Equation (1) is first solved to obtain a stationary distribution function. To lowest order in the Larmor radius expansion one obtains

$$F = F(\psi, \epsilon, \mu). \tag{2}$$

In particular for electrons and bulk ions a local Maxwellian distribution is chosen

$$F = \frac{N(\psi)}{\left(\pi v_{th}^2(\psi)\right)^{3/2}} \exp\left(-2\frac{\epsilon}{v_{th}^2(\psi)}\right), \tag{3}$$

with density N and thermal velocity squared $v_{th}^2 = 2T/m$. For the fast particles a slowing-down distribution is assumed [2]

$$F = N(\psi)\frac{C(\psi)}{v^3 + v_c^3(\psi)}H(v_0 - v), \tag{4}$$

$$v_c = \left(3\sqrt{\pi}\frac{m_f + m_i}{m_f m_i}m_e\right)^{1/3}\left(\frac{T_e}{m_e}\right)^{1/2}, \tag{5}$$

$$C = \frac{3}{4\pi \ln\left[\left(\frac{v_0}{v_c}\right)^3 + 1\right]}, \tag{6}$$

where H is the Heaviside function and v_0 the birth velocity of the fast particles ($v_0 = 1.3 \cdot 10^7 m/s$ for fusion alphas).

The linearized DKE is then solved to obtain the fluctuating part of the distribution function in terms of the EM fields

$$\left(\frac{\partial}{\partial t} + \vec{v}_{g0} \cdot \frac{\partial}{\partial \vec{X}}\right)\tilde{f} = -\left(\tilde{\vec{v}}_g \cdot \frac{\partial}{\partial \vec{X}} + \frac{\tilde{d\epsilon}}{dt}\frac{\partial}{\partial \epsilon}\right) f_0, \tag{7}$$

where

$$\vec{v}_{g0} = v_{\|}\,\vec{e}_{\|} + \vec{v}_{d0}, \tag{8}$$

$$\tilde{\vec{v}}_g = v_{\|}\frac{\vec{B}_\perp}{B_0} + \frac{\vec{E} \times \vec{B}_0}{B_0^2}, \tag{9}$$

$$\frac{\tilde{d\epsilon}}{dt} = \frac{q}{m}\,\vec{v}_{g0} \cdot \vec{E} + \mu\frac{\partial B_{\|}}{\partial t}. \tag{10}$$

As the unperturbed system is homogeneous in time and the toroidal direction, one can consider fluctuating quantities of the form $\exp i[n\varphi - (\omega + i\eta)t]$, where $\eta > 0$ ensures causality. Equation (7) is solved using a perturbation method. The operator $\vec{v}_{d0} \cdot \nabla = \mathcal{O}(\varepsilon)$, on the left hand side is considered as perturbative. Furthermore, to avoid an integration along the field line, the differential operator $\vec{e}_{\|} \cdot \nabla$, is replaced by its magnetic-surface-averaged value $< \nabla_{\|} >= ik_{\|}$, where

$$k_{\|}^2 = \frac{\oint_{\psi=const} dl\left(|\nabla_{\|}E_n|^2 + |\nabla_{\|}E_b|^2\right)}{\oint_{\psi=const} dl\,|\,\vec{E}\,|^2}, \tag{11}$$

The integrals in Eq.(11) are evaluated along a closed path in the poloidal plane on a $\psi = const$ surface. Another possibility instead of using Eq. (11) would be to make the

rough approximation $\omega^2 = v_A^2 k_\parallel^2$, since TAEs are Alfvén waves. But $k_\parallel$ obtained in this way can be wrong by a factor up to 3. The reason is the "sidebands" created by toroidal coupling: simple models give resonances at one third of the Alfvén speed.

Solving to second order in ε and retaining only the most dominant element among comparable terms leads to

$$\begin{aligned}\tilde{f} &= \frac{-iq}{m\omega_c\Omega_0}\left\{\frac{1}{\omega}\left(\Omega_0 E_b - iv_\parallel \nabla_p E_\parallel\right)\nabla_n F\right. \\ &+\left[\omega_c v_\parallel E_\parallel + \left(\frac{v_\perp^2}{2}+v_\parallel^2\right)\vec{\beta}_\perp\cdot\vec{E} - i\omega\frac{v_\perp^2}{2}B_\parallel\right]\frac{\partial F}{\partial \epsilon} \\ &\left.-i\frac{1}{\omega\omega_c}\left(\frac{v_\perp^2}{2}+v_\parallel^2\right)(\vec{\beta}_\perp\cdot\nabla)E_b\nabla_n F\right\},\end{aligned} \tag{12}$$

where $\omega_c = qB_0/m$, $\Omega_0 = \omega + i\eta - k_\parallel v_\parallel$ and $\vec{\beta}_\perp = \left(\nabla\times\vec{e}_\parallel\right)_\perp$.

One can now derive the power absorption formula. The total power exchanged between the particles and the perturbing EM fields averaged over time reads

$$P_{species} = \frac{1}{2}\Re e\int d\Gamma\,\frac{\tilde{d\epsilon}}{dt}\tilde{f}^*_{species}, \qquad d\Gamma = d^3X d^3v. \tag{13}$$

Inserting Eqs (10) and (12) leads to the following relations

$$P_{species} = P^{homo}_{species} + P^{inhomo}_{species}, \tag{14}$$

$$P^{homo} = \frac{1}{2}\Im m\int d\Gamma\frac{q^2}{m\Omega_0}\left|v_\parallel E_\parallel + \frac{1}{\omega_c}\left(\frac{v_\perp^2}{2}+v_\parallel^2\right)(\vec{\beta}_\perp\cdot\vec{E}) - i\frac{\omega}{\omega_c}\frac{v_\perp^2}{2}B_\parallel\right|^2\frac{\partial F}{\partial\epsilon}, \tag{15}$$

$$\begin{aligned}P^{inhomo} = &-\frac{1}{2}\Re e\int d\Gamma\frac{q^2}{m\omega\omega_c\Omega_0}\left[v_\parallel E_\parallel + \frac{1}{\omega_c}\left(\frac{v_\perp^2}{2}+v_\parallel^2\right)\vec{\beta}_\perp\cdot\vec{E} - i\frac{\omega}{\omega_c}\frac{v_\perp^2}{2}B_\parallel\right]\times \\ &\left[\frac{1}{\omega_c}\left(\frac{v_\perp^2}{2}+v_\parallel^2\right)(\vec{\beta}_\perp\cdot\nabla)E_b^* + v_\parallel\nabla_p E_\parallel^*\right]\nabla_n F.\end{aligned} \tag{16}$$

The resonant denominator can be written as

$$\frac{1}{\Omega_0} = \frac{1}{\omega - k_\parallel v_\parallel + i\eta} = \mathcal{P}\frac{1}{\omega - k_\parallel v_\parallel} - i\pi\frac{1}{|k_\parallel|}\delta\left(v_\parallel - \frac{\omega}{k_\parallel}\right). \tag{17}$$

Globally, only the resonant particles can exchange energy with the EM fields. The principle value in the above relation can therefore be discarded when evaluating the absorbed power.

For a Maxwellian distribution the power reads

$$P^{homo} = \sqrt{\pi}\epsilon_0 \int d^3x \frac{\omega_p^2 v_{th}}{4\omega_c^2 |k_{||}|} \exp(-z_0^2) \times \left\{ \left| 2z_0 \frac{\omega_c}{v_{th}} E_{||} + \left(1 + 2z_0^2\right) \vec{\beta_\perp} \cdot \vec{E} - i\omega B_{||} \right|^2 + \left| \vec{\beta_\perp} \cdot \vec{E} - i\omega B_{||} \right|^2 \right\}, \tag{18}$$

$$P^{inhomo} = \sqrt{\pi}\epsilon_0 \Im m \int d^3x \nabla'_n \frac{\omega_p^2 v_{th}^3}{8\omega\omega_c^3 |k_{||}|} \exp(-z_0^2) \left\{ \left[2z_0 \frac{\omega_c}{v_{th}} E_{||} + \left(1 + 2z_0^2\right) \vec{\beta_\perp} \cdot \vec{E} - i\omega B_{||} \right] \times \left[\left(1 + 2z_0^2\right) (\vec{\beta_\perp} \cdot \nabla E_b^*) + 2z_0 \frac{\omega_c}{v_{th}} \nabla_p E_{||}^* \right] + \left[\vec{\beta_\perp} \cdot \vec{E} - i\omega B_{||} \right] (\vec{\beta_\perp} \cdot \nabla) E_b^* \right\}, \tag{19}$$

where $\omega_p^2 = Nq^2/m\epsilon_0$, $z_0 = \omega/k_{||}v_{th}$ and ∇'_n is equivalent to ∇_n except that it operates only on density and temperature. For the slowing-down distribution resonant particles can exist only if the phase velocity is below the birth velocity ($|v_p = \omega/k_{||}| < v_0$), in that case

$$P^{homo} = \pi^2 \epsilon_0 \int d^3x \frac{\omega_p^2 C}{|k_{||}|} \left\{ \frac{1}{|v_p|^3 + v_c^3} \left| v_p E_{||} + \frac{1}{\omega_c} v_p^2 \vec{\beta_\perp} \cdot \vec{E} \right|^2 + \frac{2I_0}{\omega_c} \Re e \left(\vec{\beta_\perp} \cdot \vec{E}^* + i\omega B_{||}^* \right) \left(v_p E_{||} + \frac{v_p^2}{\omega_c} \vec{\beta_\perp} \cdot \vec{E} \right) + \frac{I_1}{\omega_c^2} \left| \vec{\beta_\perp} \cdot \vec{E} - i\omega B_{||} \right|^2 \right\}, \tag{20}$$

$$P^{inhomo} = -\pi^2 \epsilon_0 \Im m \int d^3x \nabla'_n \frac{\omega_p^2 C}{|k_{||}|\omega_c} \left\{ I_0 \left(v_p E_{||}^* + \frac{v_p^2}{\omega_c} \vec{\beta_\perp} \cdot \vec{E}^* \right) \left(\frac{v_p^2}{\omega\omega_c} (\vec{\beta_\perp} \cdot \nabla) E_b + \frac{\nabla_p E_{||}}{k_{||}} \right) + \frac{I_1}{2\omega_c} \left[\left(\vec{\beta_\perp} \cdot \vec{E}^* + i\omega B_{||}^* \right) \left(\frac{v_p^2}{\omega\omega_c} (\vec{\beta_\perp} \cdot \nabla) E_b + \frac{\nabla_p E_{||}}{k_{||}} \right) + \frac{1}{\omega} (\vec{\beta_\perp} \cdot \nabla) E_b \left(v_p E_{||}^* + \frac{v_p^2}{\omega_c} \vec{\beta_\perp} \cdot \vec{E}^* \right) \right] + \frac{I_2}{4\omega\omega_c^2} (\vec{\beta_\perp} \cdot \nabla) E_b \left(\vec{\beta_\perp} \cdot \vec{E}^* + i\omega B_{||}^* \right) \right\}, \tag{21}$$

$$\text{where} \quad I_n = \int_{|v_p|}^{v_0} dv \frac{v \left(v^2 - v_p^2\right)^n}{v^3 + v_c^3}. \tag{22}$$

If the EM fields are calculated from an ideal MHD model as in the code LION [3], $E_{||}$ is zero. In that case $E_{||}$ must be obtained from a more general model. The starting point is the quasi-neutrality condition

$$\tilde{N}_e = \tilde{N}_i \,. \tag{23}$$

As the thermal velocity of the electrons can be comparable to the phase velocity ($v_{the} \sim |v_p|$), it is reasonable to evaluate the dominant term of $\tilde{N}_e$ using a kinetic model. For this reason $\tilde{f}_{electron}$ is integrated over velocity and leads to

$$\tilde{N}_e = 2i\frac{eN_e}{m_e\omega\omega_{ce}}\left[\frac{\omega\omega_{ce}}{k_{\|}v_{the}^2}(1-Z)E_{\|} - \frac{1}{2}Z\left(\vec{\beta}_{\perp}\cdot\vec{E}_{\perp} - i\omega B_{\|}\right) + \left(\frac{\omega}{k_{\|}v_{the}}\right)^2(1-Z)\,\vec{\beta}_{\perp}\cdot\vec{E}\right], \tag{24}$$

where $Z \equiv Z\left(\frac{\omega}{|k_{\|}|v_{the}}\right)$ is the plasma dispersion function [4]. However, to evaluate $\tilde{N}_i$ one can use a cold fluid model for the ions as $v_{thi} \ll |v_p|$. Due to their relatively large mass, the ions dominate the motion perpendicular to the magnetostatic field. Solving the equation of motion in the perpendicular plane, one obtains for low frequencies $\omega \ll \omega_{ci}$

$$\vec{v} = \frac{e}{m_i\omega_{ci}}\left[\vec{E}_{\perp}\times\vec{e}_{\|} - i\frac{\omega}{\omega_{ci}}\vec{E}_{\perp}\right], \tag{25}$$

and using the equation of continuity for the ion density gives

$$\tilde{N}_i = -\frac{eN_i}{m_i\omega_{ci}^2}\left[\nabla\cdot\vec{E}_{\perp} - 2i\frac{\omega_{ci}}{\omega}\vec{\beta}_{\perp}\cdot\vec{E}_{\perp} - \omega_{ci}B_{\|}\right]. \tag{26}$$

Inserting these density relations in the quasi-neutrality condition leads to

$$E_{\|} = -\frac{k_{\|}v_{the}^2}{2\omega\omega_{ce}}\left\{\frac{1}{1-Z}\left(i\frac{\omega}{\omega_{ci}}\nabla\cdot\vec{E}_{\perp} + \vec{\beta}_{\perp}\cdot\vec{E}_{\perp}\right) + \left[1 + 2\left(\frac{\omega}{k_{\|}v_{the}}\right)^2\right]\vec{\beta}_{\perp}\cdot\vec{E}_{\perp} - i\omega B_{\|}\right\}. \tag{27}$$

Finally, using the above expression in the power relation for electrons and ions gives

$$P^{homo} = \sqrt{\pi}\epsilon_0\int d^3x\frac{\omega_p^2 v_{th}}{4\omega_c^2|k_{\|}|}\exp -z_0^2 \times \left(|a_{species}|^2 + \left|\vec{\beta}_{\perp}\cdot\vec{E} - i\omega B_{\|}\right|^2\right), \tag{28}$$

$$a_{electron} = \frac{1}{1-Z}\left(i\frac{\omega}{\omega_{ci}}\nabla\cdot\vec{E}_{\perp} + \vec{\beta}_{\perp}\cdot\vec{E}_{\perp}\right), \tag{29}$$

$$\begin{aligned} a_{ion} = {} & \frac{T_e}{T_i}\frac{1}{1-Z}\left(i\frac{\omega}{\omega_{ci}}\nabla\cdot\vec{E}_{\perp} + \vec{\beta}_{\perp}\cdot\vec{E}_{\perp}\right) - i\omega\left(1+\frac{T_e}{T_i}\right)B_{\|} \\ & + \left[1 + \frac{T_e}{T_i} + 2\left(\frac{\omega}{k_{\|}v_{thi}}\right)^2\right]\vec{\beta}_{\perp}\cdot\vec{E}_{\perp}\,. \end{aligned} \tag{30}$$

P^{inhomo} can be neglected for these species. This is related to the fact that in the frame of the present work $\omega \gg \omega^\star$ for electrons and ions, where $\omega^\star$ is the characteristic frequency of the drift mode.

Note that the contributions of $E_{||}$ to the power absorbed by the ions are proportional to T_e/T_i. As the average kinetic energy of the fast particles is very high as compared with the energy of the electrons, the contributions of $E_{||}$ to the power absorbed by the fast particles can therefore be neglected. In this way, one can write for the fast particles

$$\begin{aligned} P_f^{homo} &= \pi^2\epsilon_0 \int d^3x \frac{\omega_{pf}^2 C}{|k_{||}|\omega_{cf}^2} \left\{ \left[\frac{v_p^4}{|v_p|^3 + v_c^3} + 2v_p^2 I_0 \right] \left| \vec{\beta}_\perp \cdot \vec{E} \right|^2 \right. \\ &\left. + 2\omega v_p^2 I_0 \Im m \left(B_{||}\, \vec{\beta}_\perp \cdot \vec{E}^\star \right) + I_1 \left| \vec{\beta}_\perp \cdot \vec{E} - i\omega B_{||} \right|^2 \right\}, \end{aligned} \tag{31}$$

$$\begin{aligned} P_f^{inhomo} &= \frac{\pi^2\epsilon_0}{\omega} \Im m \int d^3x \nabla'_n \frac{\omega_{pf}^2 C}{|k_{||}|\omega_{cf}^3} \left\{ \left(v_p^4 I_0 + v_p^2 \frac{I_1}{2} \right) \vec{\beta}_\perp \cdot \vec{E} \right. \\ &\left. + \left(v_p^2 \frac{I_1}{2} + \frac{I_2}{4} \right) \left(\vec{\beta}_\perp \cdot \vec{E} - i\omega B_{||} \right) \right\} (\vec{\beta}_\perp \cdot \nabla) E_b^\star. \end{aligned} \tag{32}$$

The expressions (28)-(32) have been written in toroidal axisymmetric geometry and implemented in the LION code.

Acknowledgments

This work was partly supported by the Swiss National Science Foundation.

References

[1] VILLARD, L., BRUNNER, S., VACLAVIK, J., Theoretical aspects of effects of high-energy particles on MHD modes, in these proceedings

[2] KOCH, R., Phys.Lett. A **157**, (1991) 399.

[3] VILLARD, L., APPERT, K., GRUBER, R., VACLAVIK, J., Comput.Phys.Rep. **4** (1986) 95.

[4] SHAFRANOV, V.D., in Reviews of Plasma Physics, edited by M.A.Leontovich (Consultants Bureau, New York, 1967) Vol.3.

Linear Wave Propagation in resistive/hot Tokamak Plasmas

A. Jaun, K. Appert, H.Lütjens*, J.Vaclavik and L.Villard

Centre de Recherches en Physique des Plasmas,
Association Euratom–Confédération Suisse,
Ecole Polytechnique Fédérale de Lausanne
*CPT Ecole Polytechnique, Palaiseau (France)

1 ABSTRACT

Using the bicubic finite element codes CHEASE and PENN, Maxwell's equations are solved for global wavefields in a realistic tokamak equilibrium.

Two different models have been implemented to calculate the linear response of the plasma: a cold resistive model which gives results in good agreement with the cold toroidal code LION in the case of TAE mode computations. The second is a hot kinetic model, which is validated with the hot cylindrical code ISMENE, reproducing the mode conversion to a kinetic Alfvén wave in the large aspect ratio limit.

Using the new tool for a preliminary study, self-consistent (non-perturbative) calculations of TAE mode wavefields show how finite Larmor radius effects can couple a gap mode to the kinetic Alfvén wave, resulting in a radiatively damped KTAE mode.

2 INTRODUCTION

Among the important questions to be solved in magnetic fusion the excitation, propagation and damping of waves plays an essential role. While the wave excitation and absorption can be used to heat the plasma, unstable modes may grow from the energy of the particles, resulting in rapid reorganizations of the plasma equilibrium and subsequent loss of confinement.

If the wavelengths of the perturbations are comparable to the dimensions of the device, the global nature of the waves has to be taken into account explicitly; this has led for example to the toroidal codes LION [1] and CASTOR [2] which determine the

the Alfvén resonance, resulting in a conversion of the energy from one to the other. The qualitative picture of the fluid model which predicts a singular behavior of the fields at the Alfvén resonance is then different in the hot model, where the singularity is replaced by a conversion to the short wavelength kinetic Alfvén (KAW) wave or the quasi-electrostatic surface wave (SQEW) [3]. The continuum damping obtained in the fluid approximation can be different from the corresponding kinetic damping. This happens when the emitted kinetic wave is so weakly damped that it appears as a standing wave. An intrinsically kinetic effect which does not have a fluid counterpart is known as "radiative damping"; it also consists of a coupling of the gap mode to kinetic modes.

Another example where the wavefield structure and the energy deposition cannot be calculated from the fluid models is found in the ICRF range of frequencies. The conversion of the fast magnetosonic wave to an ion Bernstein wave at the ion-ion hybrid resonance can only be described by models including FLR effects.

Motivated by these examples, the new toroidal code PENN has been developed, taking into account FLR effects up to second order in $k_\perp \rho_L$ where $k_\perp$ is the transverse wave vector and ρ_L the Larmor radius of the species. This allows for a non-perturbative treatment of the kinetic waves such as the kinetic Alfvén and the ion Bernstein waves.

After a short description of the new model, this paper shows validations in two limiting cases: the cold and hot-plasma models in fully toroidal and cylindrical geometry, respectively. In the first case, waveforms and eigenfrequencies of TAE gap modes in a realistic DIII-D equilibrium are compared with those obtained with the LION code. In the second case, an Alfvén wave heating scenario exhibiting wave conversion is computed in the large aspect ratio limit and compared with results from the cylindrical code ISMENE [3].

Confident with these validations, preliminary results are then given for kinetic calculations in a low aspect ratio equilibrium, showing how a TAE mode might be modified by FLR effects.

3 MODEL

The wave propagation problem which is under discussion here consists in the resolution of Maxwell's equations in a medium where the linear response to a field perturbation is determined by the dielectric tensor $\overleftrightarrow{\epsilon}$.

A straightforward finite elements discretization of Maxwell's operator in terms of the electric field results in additional unphysical solutions which have disastrous effects in the range of frequencies we consider: gap mode calculations would find the global physical modes as well as a high number of numerically produced spurious modes, with no easy way to distinguish the ones from the others. This phenomenon is called "spectral pollution" [4]. This problem can be solved by using a Fourier decomposition in the poloidal direction [2], or with a discretization based on 2D finite hybrid elements [1], [5]. The linear hybrid finite elements used so far are, however, insufficient to discretize

operators involving up to 4th order derivatives, and no straightforward generalization exists for cubic hybrid elements.

An elegant way to avoid the problem related to the spectral pollution consists in writing Maxwell's operator in terms of the electromagnetic potentials $(\vec{A}, \Phi)$ [6], [7]:

$$\begin{cases} \vec{\nabla}^2\vec{A} + \left(\frac{\omega}{c}\right)^2 \overleftrightarrow{\epsilon} \cdot \vec{A} + i\left(\frac{\omega}{c}\right) \overleftrightarrow{\epsilon} \cdot \vec{\nabla}\,\phi &= -\frac{4\pi}{c}\,\vec{j_{ext}} \\ \vec{\nabla} \cdot \left(\overleftrightarrow{\epsilon} \cdot \vec{\nabla}\,\phi\right) - i\left(\frac{\omega}{c}\right) \vec{\nabla} \cdot \left(\overleftrightarrow{\epsilon} \cdot \vec{A}\right) &= 0 \end{cases} \tag{1}$$

where the Coulomb gauge has been used explicitly and has to be further imposed on the domain boundaries. ω is the excitation frequency of the antenna source currents which are chosen such as to satisfy the condition $\vec{\nabla} \cdot \vec{j_{ext}} = 0$.

In order to separate the plasma response along the static magnetic field from the one across, it is advantageous to introduce the local unit vectors $(\vec{e_n}, \vec{e_b}, \vec{e_\parallel})$ such that $\vec{e_n} = \vec{\nabla}\,\Psi / \| \vec{\nabla}\,\Psi \|, \vec{e_b} = \vec{e_\parallel} \times \vec{e_n}, \vec{e_\parallel} = \vec{B_0}\,/B_0$, where Ψ is the flux function defining a Grad-Shafranov equilibrium. The dielectric tensor for the cold resistive plasma model can then be derived [3] from the standard resistive two fluid theory as

$$\overleftrightarrow{\epsilon}^{cold} = 1 + \begin{pmatrix} \epsilon_1 & i\epsilon_2 + \mu[\beta_{12} - \nabla_\parallel] & 0 \\ -i\epsilon_2 + \mu[\beta_{21} + \nabla_\parallel] & \epsilon_1 + \mu\beta_{22} & 0 \\ 0 & 0 & \epsilon_3 \end{pmatrix} \tag{2}$$

$$\epsilon_1 = \left(\frac{c}{c_A}\right)^2 \frac{\Omega_{ci}^2}{\Omega_{ci}^2 - \omega^2} \qquad \epsilon_2 = i\left(\frac{\omega}{\Omega_{ci}}\right)\epsilon_1 \qquad \epsilon_3 = i\frac{\omega_{pe}^2}{\omega\nu_{ei}}$$

$$\mu = \left(\frac{c}{\omega}\right)^2 \beta_{33} \qquad \beta_{ij} = \vec{e_j} \cdot \vec{\nabla} \times \vec{e_i}$$

Note that the finite electron mass has been neglected here, resulting in a change $\epsilon_3 = -\frac{\omega_{pe}^2}{\omega(\omega + i\nu_{ei})} \longrightarrow i\frac{\omega_{pe}^2}{\omega\nu_{ei}}$ so as to avoid the SQEW wave [3] which does not exist in the model used in the code LION. Here $c, \Omega_{ci}, \omega_{pe}$ and ν_{ei} have the standard meaning and c_A is the Alfvén speed.

The kinetic model [8] has been derived directly from the linearized Vlasov equation assuming a Maxwellian distribution of the species. It takes into account FLR effects up to second order in $k_\perp \rho_L$ and equilibrium gradients up to first order in ρ_L/L, L being a characteristic length of the equilibrium. The dispersion and damping resulting from the Maxwellian distribution of the particles are expressed in terms of the dispersion function Z. All this is summarized symbolically here by the expression:

$$\overleftrightarrow{\epsilon}^{kinetic} = 1 + \sum_\alpha \overleftrightarrow{\epsilon}_\alpha \left(\vec{\nabla}^2, \vec{\nabla}, Z\left(\frac{\omega - l\Omega_{c\alpha}}{|k_\varphi| v_\alpha^{th}}\right)\right) \tag{3}$$

The working coordinates are chosen as $(s = \sqrt{\Psi/\Psi_s}, \theta, \varphi)$, where the radial variable s labels the flux surface whereas θ and φ are the standard polar and toroidal angles

respectively. Ψ_s is the flux at the plasma-vacuum interface. Solving Maxwell's equations (eq.1) in terms of the perturbed potentials $(\vec{A}, \Phi)$ and computing the fields $(\vec{E}, \vec{B})$ by simple differentiation, it is possible to define the power absorbed by the plasma P^{Pla}, the normal Poynting flux S_n, the vacuum power P^{vac} and the power emitted by the antenna P^{ant} as

$$P^{pla}(s) = \frac{\omega}{8\pi} \int_0^{2\pi} d\theta \int_0^s ds |J| (\| \vec{B} \|^2 - \vec{E}^* \cdot \overleftrightarrow{\epsilon} \cdot \vec{E}) \tag{4}$$

$$S_n(s) = \frac{c}{8\pi} \int_0^{2\pi} d\theta \| J \vec{\nabla} s \| (\vec{E}^* \times \vec{B})_n \tag{5}$$

$$P^{vac} = \frac{\omega}{8\pi} \int_{vac} dV (\| \vec{B} \|^2 - \| \vec{E} \|^2) \tag{6}$$

$$P^{ant} = -\frac{\omega}{2c} \int_{ant} dV \, \vec{j_{ext}} \cdot \vec{A}^* \tag{7}$$

where J is the Jacobian. For the resistive model for the plasma, it is possible to check the balance of powers all over the plasma radius $s \in [0; 1]$ according to

$$iS_n(s) = P^{pla}(s) \tag{8}$$

A local power balance cannot in general be defined for the hot plasma model. It is however possible to check the consistency of the solution at the plasma-vacuum interface using the power balance

$$P^{vac} + P^{ant} = iS_n(s = 1) \tag{9}$$

4 NUMERICAL IMPLEMENTATION

In order to compute wavefields in situations relevant for experiments, an interface has been developed with the equilibrium code CHEASE [9], which solves the Grad-Shafranov equation using arbitrary pressure and current profiles. The smooth solution, provided by the Hermite bicubic finite element discretization further processed with a cubic spline smoothing, guarantees a good representation of second derivatives of the equilibrium quantities.

A mesh is further extended in the vacuum region to the wall, which is chosen here to be at a constant distance of the plasma edge.

The 4th order partial differential equations (eq.1) are also discretized with Hermite bicubic finite elements. The standard procedure is used, choosing the same elements for the basis and the test functions in the weak variational form corresponding to (eq.1). The finiteness of the solution on the axis and the Coulomb gauge at the boundary are imposed naturally through the variational form. On the axis, the electrostatic potential is chosen

to be zero and the vector character of $\vec{A}$ and $\vec{\nabla}\ \phi$ is imposed explicitly. The essential boundary conditions on the perfectly conducting wall reduce to vanishing tangential components of $\vec{A}$ and $\vec{\nabla}\ \phi$.

5 VALIDATIONS

Two types of comparison are shown here: one using the cold resistive model (eq.2) in an up/down asymmetric elongated single null equilibrium typical of DIII-D, comparing eigenfrequencies and wavefields of TAE gap modes with the results obtained using the finite hybrid element code LION [1]. This is a strong check for the discretization of Maxwell's operator in a complicated geometry. The second check is performed using the kinetic model (eq.3) in a circular cross-section and large aspect ratio limit. An Alfvén wave conversion scenario is reproduced and the wavefields are compared with the hot cylindrical code ISMENE [3]. This leaves only a part of the terms which are toroidal and kinetic unchecked, as the kinetic expressions have to combine in a rather sophisticated way to recover the cylindrical limit.

Using the cold resistive model (eq.2), a scan in frequency in the gap region shows two peaks in the antenna load, identified as two TAE modes at 41.5 and 70.5$[kHz]$. This is in good agreement with a similar calculation performed with the code LION, which situates the modes at 42.4 and 69.1$[kHz]$. A comparison of the wavefields shows excellent agreement in the dominant component E_n as well as in the weaker component E_b which is shown in fig.1 for the higher frequency mode. Note that the fields shown

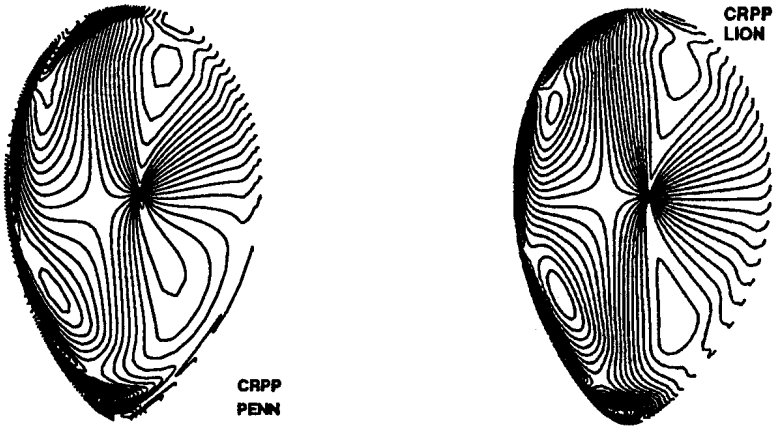

Figure 1: *Level line plots for Re(Eb) with 5% damping in PENN and 1% in LION. Other parameters are* $R_0 = 1.8m, R/a = 2.77, \kappa = 1.63, q_0 = 1.1, q_a = 3.1, \beta = 1.1\%, \beta_{pol} = 0.19, B_0 = 0.741T, I_p = 1MA, n_{e0} = 4.1.10^{19}(1 - 0.9s^2)^{0.5}m^{-3}$

here are independent of the antenna shape and position and reflect only the eigenmode structure.

As a check for the numerical consistency of the solution, the local power balance (eq.8) is computed from the plasma center to the wall. The power absorption is strongly localized near the plasma edge as can be seen in fig.2 (right); the numerical resolution

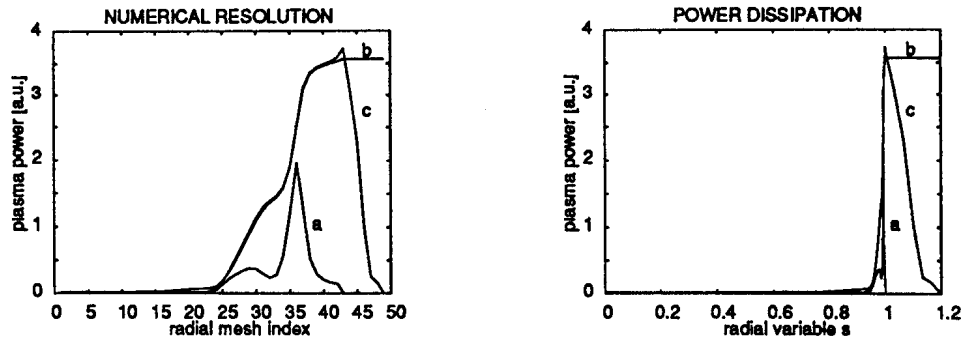

Figure 2: *Self-consistency check showing (a) the local resistive dissipation, (b) the power integrated from the center $Im(P^{Pla})$ and (c) the normal Poynting flux $Re(S_n)$ plotted versus the radial variable s (right) and the radial mesh index (left).*

was nonetheless sufficient thanks to a packing of the radial mesh near the plasma edge resolving the skin depth and the structure of the mode (fig.2, left). The agreement between the local powers (eq.8) is better than 1.6 % all over the plasma radius, while the balance checked at the plasma edge (eq.9) is better than 1.9 %.

A good check of the hot model (eq.3) can be performed in the large aspect ratio limit, computing the wavefields in an Alfvén wave heating scenario where the fast magnetosonic wave converts to a kinetic Alfvén wave. Using the 1D cubic finite element code ISMENE with a radial resolution $N_s = 100$ and assuming a poloidal mode $m = -1$, it is possible to compare the fields obtained with PENN in 2D using a helical antenna excitation $m = -1$, here with a numerical resolution $N_s = 18, N_\theta = 18$:

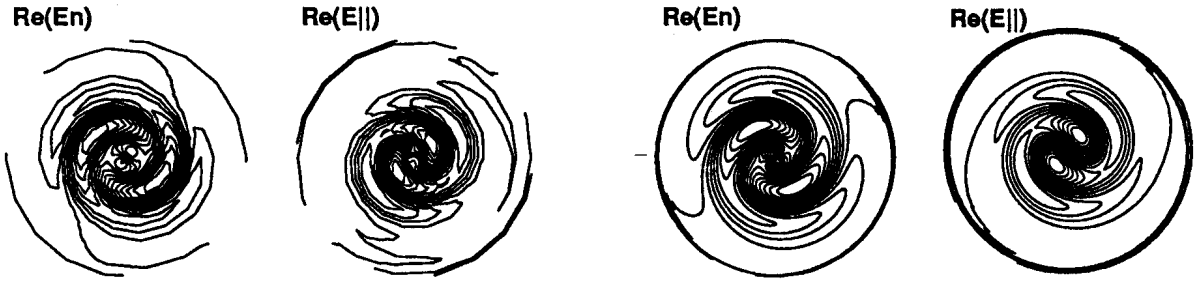

Figure 3: *Level line plots for $Re(E_n)$ and $Re(E_\parallel)$ using PENN (left) and ISMENE (right). The parameters correspond to a large aspect ratio model for the TCA tokamak with $f = 3MHz, q_0 = 1.1, q_a = 3.3, I_p = 112kA, B_0 = 1.5T, \beta = 0, n_{e0} = n_{D0} = 3.10^{19}m^{-3}, T_{e0} = 800eV, T_{i0} = 500eV, n = n_0(1 - 0.98s^2)^{0.7}, T = T_0(1 - 0.84s^2)^2$*

ACKNOLEDGEMENTS

This work was supported in part by the Swiss National Science Foundation.

References

[1] L.Villard, K.Appert, R.Gruber, J.Vaclavik, *Comput.Phys.Reports.* **4** (1986) 95

[2] W.Kerner, S.Poedts, J.P.Goedbloed, G.T.A.Huysmans, B.Keegan, E.Schwarz, *Proc. 18th European Conf. on Controlled Fusion and Plasma Physics (Berlin 3-7 June 1991)* pp IV.89-IV.92

[3] J.Vaclavik, K.Appert, *Nucl.Fusion* **31** (1991) 1945

[4] K. Appert, D. Berger, R. Gruber, F. Troyon, and J. Rappaz, *J. Appl. Math. Phys. (ZAMP)* vol. 25 pp. 229-240, 1974

[5] R. Gruber, F. Troyon, D. Berger, L.C. Bernard, S. Rousset, R. Schreiber, W. Kerner, W. Schneider, K.V. Roberts, "ERATO stability code", *Comput. Phys. Commun*, vol. 21, pp. 323-371, 1981

[6] D.B. Batchelor, E.F. Jaeger and H. Weitzner, "2D full wave modeling of ICRF with finite parallel electric field", *Theory of Fusion Plasmas (Proc. Int. Workshop, Varenna, 1988) Editrice Compositori, Bologna (1988)*

[7] A.Jaun, K.Appert, J.Vaclavik, Lausanne report LRP 492/94 (1994)

[8] S.Brunner, J.Vaclavik, *Phys. Fluids B* **5** (1993) 1695

[9] H.Lütjens, A.Bondeson, A.Roy, *Comput.Phys.Commun.* **69** (1992) 287

3-D FOKKER-PLANCK CODE VALID FOR ARBITRARY COLLISIONALITY AND ADJOINT FUNCTION FOR BOOTSTRAP CURRENT CALCULATION

O. Sauter[a], Y. R. Lin-Liu[b], F. L. Hinton[b], and J. Vaclavik[a]

a) Centre de Recherches en Physique des Plasmas
Association Euratom - Confédération Suisse
Ecole Polytechnique Fédérale de Lausanne
21, Av. des Bains, CH-1007 Lausanne, Switzerland

b) General Atomics, San Diego, USA

Abstract

We have developed a 3-D code, CQL$_{//}$ [1], which solves the drift-kinetic Fokker-Planck equation along the magnetic field line on a given flux surface. It is 2-D in velocity space and 1-D spatially along **B**. Therefore no bounce-averaging is performed and the model is valid for arbitrary collisionality and axisymmetric tokamak equilibria. The adjoint function formalism has been adapted to calculate the neoclassical bootstrap current, assuming small banana width compared with the minor radius. We compare the results of our code with published analytical formulae and with the results of the modified bounce-averaged code CQL3D.

1. Introduction

The neoclassical transport coefficients and in particular those for the bootstrap current are widely used for data analysis or for MHD equilibrium calculations with large fraction of bootstrap current. Analytical formulae exist [2-6], but they are valid either at low collisionality ($\nu_e^* < 10^{-3}$) or at low inverse aspect ratio ε. Bounce-averaged Fokker-Planck code, such as CQL3D [7] or ADJ [8], can be used to obtain these coefficients for arbitrary ε and realistic axisymmetric tokamak geometry. Considering only the pitch-angle scattering collision operator, the code DKES [9] solves for arbitrary collisionality in a stellerator type configuration. The aim of CQL$_{//}$, is to solve the Fokker-Planck equation with the full collision operator, including like-species collisions. In this way, no conditions on the ratio of the collision frequency to the bounce frequency is assumed and the transport coefficients can be determined for arbitrary ν_e^*. In this paper, we present the adjoint function formalism used to easily calculate these coeffficients for the bootstrap current [10]. We also compare our results with analytical formulae.

2. Basic equations and bootstrap current coefficients

Using the adjoint function formalism [11,12], we shall obtain the parallel current determined by the perturbed distribution function solution of the linearized Fokker-Planck equation written as follows (Eq.5.21-24 Ref.2):

$$v_{//}\,\hat{b}\cdot\nabla f_{e1} - C_e^l(f_{e1}) = -(v_D\cdot\nabla\psi)_e \frac{\partial f_{e0}}{\partial\psi} + \frac{q_e}{T_e} v_{\|} f_{e0} E_{\|}^O \tag{1}$$

$$v_{//}\,\hat{b}\cdot\nabla f_{i1} - C_{ii}^l(f_{i1}) = -(v_D\cdot\nabla\psi)_i \frac{\partial f_{i0}}{\partial\psi} \tag{2}$$

with

$C_e^l = C_{ee}^l + C_{ei}^l$: Linearized collision operator (Rosenbluth potentials)

$$(v_D\cdot\nabla\psi)_\sigma = I(\psi)\, v_{//}\, \hat{b}\cdot\nabla\left(\frac{v_{//}}{\Omega_\sigma}\right)$$

$$\frac{\partial f_{\sigma 0}}{\partial\psi} = f_{\sigma 0}\left[\frac{\partial \ln n_{\sigma 0}}{\partial\psi} + \frac{q_\sigma}{T_\sigma}\frac{\partial\langle\Phi\rangle}{\partial\psi} + \left(\frac{v^2}{v_{T\sigma}^2} - \frac{3}{2}\right)\frac{\partial \ln T_{\sigma 0}}{\partial\psi}\right]$$

$E_{//}^O$: Ohmic parallel electric field ; $I(\psi) = R B_\phi$,

and where $v_{T\sigma}^2 = 2T^2/m_\sigma$ and $\Omega_\sigma = q_\sigma B_0/m_\sigma$ are the thermal velocity and cyclotron frequency of species σ. We then introduce the following transformation, where $u_{i//}$ is the ion parallel flow:

$$g_{e1} = f_{e1} - \frac{2\, v_{//}\, u_{i//}}{v_{T\sigma}^2} f_{e0} + \sum_k \alpha_k A_k f_{e0} \tag{3}$$

with

$$\begin{aligned}
&A_1 = \frac{1}{p_e}\frac{\partial p_e}{\partial\psi} + \frac{1}{p_e}\frac{\partial p_i}{\partial\psi}\ ;\ \alpha_1 = I(\psi)\, v_{//}/\Omega_e \\
&A_2 = \frac{1}{T_e}\frac{\partial T_e}{\partial\psi}\ ;\ \alpha_2 = \alpha_1\,(v^2/v_{T\sigma}^2 - 5/2) \\
&A_4 = \frac{q_e}{n_i T_e}\frac{K_i(\psi)}{I(\psi)}\langle B^2\rangle\ ;\ \alpha_4 = \alpha_1 B^2/\langle B^2\rangle \\
&K_i(\psi) = \frac{n_i u_{i//}}{B} + \left(\frac{\partial\langle\Phi\rangle}{\partial\psi} + \frac{1}{n_i q_i}\frac{\partial p_i}{\partial\psi}\right)\frac{I(\psi)}{B^2} n_i
\end{aligned} \tag{4}$$

In this way, Eq.(1) reduces to:

$$v_{//}\,\hat{b}\cdot\nabla g_{e1} - C_{e0}^l(g_{e1}) = S \tag{5}$$

where

$$C_{e0}^l = C_{ee}^l + \frac{\nu_{ei}(v)}{2}\frac{\partial}{\partial\xi}(1-\xi^2)\frac{\partial}{\partial\xi},\ \xi \equiv \frac{v_{//}}{v}$$

$$S = \frac{q_e E_{//}^O}{T_e} v_{//} f_{e0} - C_e^l\left(\sum \alpha_k A_k f_{e0}\right)$$

$$\nu_{ei}(v) = \frac{3\sqrt{\pi}}{4\tau_e}\frac{v_{Te}^3}{v^3}\ ;\ \frac{1}{\tau_e} = \frac{16\sqrt{\pi}}{3}\frac{n_e Z_i e^4 \ln\Lambda}{m_e^2 v_{Te}^3}\ ;\ \nu_{e^*} = \frac{\sqrt{2}\, r\, B_0}{B_{p0}\, v_{Te}\, \tau_e\, \varepsilon^{3/2}}.$$

The flux surface averaged parallel current $\langle j_{//} B \rangle$, including the ohmic and bootstrap contribution, is given by:

$$\langle j_{//} B\rangle = \langle B \int v_{//} (q_e f_{e1} + q_i f_{i1})\, d^3v \rangle$$

$$= \langle B \int q_e v_{//} g_{e1}\, d^3v \rangle - \Sigma \langle B \int q_e v_{//} \alpha_k f_{e0}\, d^3v \rangle A_k \qquad (6)$$

where we have used the quasi-neutrality condition. We now introduce the following adjoint equation obtained from the adjoint operators of the left hand-side of Eq.(5):

$$- v_{//} \hat{b}\cdot\nabla\chi_e - C^{l}_{e0}(\chi_e) = q_e v_{//} B f_{e0} \qquad (7)$$

In this way, the first term of the right-hand side of Eq.(6) becomes:

$$\langle \int g_{e1} q_e v_{//} B\, d^3v \rangle = \langle \int \frac{g_{e1}}{f_{e0}} [- v_{//} \hat{b}\cdot\nabla - C^{l}_{e0}](\chi_e)\, d^3v \rangle$$

$$= \langle \int \frac{\chi_e}{f_{e0}} [\, v_{//} \hat{b}\cdot\nabla - C^{l}_{e0}](g_{e1})\, d^3v \rangle$$

$$= \langle \int \frac{\chi_e}{f_{e0}} S\, d^3v \rangle \qquad (8)$$

where we have used the property of adjoint operators and the relation:

$$\int h\, C^{l}_{e0}(g)\, d^3v = \int \frac{g}{f_{e0}} C^{l}_{e0}(f_{e0}\, h)\, d^3v$$

Thus, once the adjoint function χ_e is known, solving Eq.(7), we can compute the parallel current simply by integrating the source term of the original equation, Eq.(6), multiplied by χ_e/f_{e0}. Using the relations given in Eq.(4) and the following definition of the transport coefficient for the current: $\langle j_{//} B\rangle = \sigma_{neo} \langle E^{O}_{//} B\rangle + L_{31} A_1 + L_{32} A_2 + L_{34} A_4$, the coefficients can be identified to:

$$\sigma_{neo} = \frac{q_e}{T_e} \langle \frac{1}{B} \int v_{//} \chi_e\, d^3v \rangle \qquad (9)$$

$$L_{31} = - I p_e - \langle \int \frac{\chi_e}{f_{e0}} C^{l}_{e0}(\alpha_1 f_{e0})\, d^3v \rangle$$

$$= - I p_e + \langle \int \chi_e Z_i \nu_{e0} \alpha_1 \frac{v^3_{Te}}{v^3} d^3v \rangle \qquad (10)$$

$$L_{32} = - \langle \int \frac{\chi_e}{f_{e0}} C^{l}_{e0}(\alpha_2 f_{e0})\, d^3v \rangle$$

$$= \langle \int \chi_e \nu_{e0} \alpha_1 [\, Z_i \frac{v^3_{Te}}{v^3} (\frac{v^2}{v^2_{Te}} - \frac{5}{2}) - h(\frac{v}{v_{Te}})]\, d^3v \qquad (11)$$

$$L_{34} = - I p_e - \langle \int \frac{\chi_e}{f_{e0}} C^{l}_{e0}(\alpha_4 f_{e0})\, d^3v \rangle$$

$$= - I p_e + \langle \int \chi_e Z_i \nu_{e0} \alpha_1 \frac{v^3_{Te}}{v^3} \frac{B^2}{\langle B^2\rangle} d^3v \rangle \qquad (12)$$

where $h(x) = x^{-3} [\, 10\, \mathrm{erf}(x) - 10\, x\, \mathrm{erf}'(x) - 4\, x^2\, \mathrm{erf}(x)]$ and $\nu_{e0} = 3\sqrt{\pi}/(4 Z_i \tau_e)$. Thus the code $CQL_{//}$ has been modifed to solve Eq.(7) and compute relations (9-12). This required the inclusion of

the linearized collision operator. We have also modifed the code CQL3D [7] to solve the bounce-averaged version of Eq.(7), which enables us to compute more rapidly the transport coefficient in the banana regime, using the bounce-averaged form of Eq.(9-12).

3. Results

We show only results for the first two coefficients, σ_{neo} and L_{31}, that is the neoclassical parallel conductivity and the contribution of the pressure gradients to bootstrap current. The superscript CQL3D or CQL$_{//}$ denotes that the corresponding coefficient has been obtained with or without bounce-averaging Eq.(7).

In Fig.1 we show $\sigma_{neo}/\sigma_{Spitzer}$ vs. $\sqrt{\varepsilon}$, with $n_e=10^{18}$ m^{-3} and T_e=3keV, in a low collisionality limit. We see that σ^{CQL3D} (solid circles) follows well Hirshman et al formula [3]. On the other hand, $\sigma^{CQL//}$ (open circles) is slightly shifted upwards and follows well Hinton and Hazeltine formula [2] (crosses), which is valid for small collisionality including $O(\backslash R(\nu_e*))$ terms, whereas Hirshman formula [3] has terms $O(\nu_e*)$. As $\nu_e*\leq 0.02$, mainly the $O(\sqrt{\nu_e*})$ terms modify the banana regime conductivity. Moreover, we have fitted the results of CQL3D in terms of f_T, the fraction of trapped particle as defined by Hirshman [5]:

$$f_T = 1 - f_c = 1 - \frac{3}{4}\langle B^2 \rangle \int_0^{1/B_{max}} \frac{\lambda\, d\lambda}{\langle (1 - \lambda B)^{1/2} \rangle} \qquad (13)$$

In this way we obtain:

$$\sigma^{CQL3D} / \sigma_{Sptz}(f_T) = F_{33}(f_T) \equiv 1 - 1.3574\, f_T + 0.5859\, f_T^2 - 0.2285\, f_T^3 , \qquad (14)$$

where we have constrained the coefficients such that $F_{33}(0) = 1$ and $F_{33}(1) = 0$, corresponding to the limits $\varepsilon \to 0$ and $\varepsilon \to 1$, respectively. Note that $F_{33}(f_T)$ would be undistinguishable from the results of CQL3D in Fig.1. Then, if we replace f_T by:

$$f_T^{eff}(\nu_e*) \equiv \frac{f_T}{1 + \sqrt{\nu_e*} + 0.25\, \nu_e*} = \frac{f_T}{(1 + 0.5\, \sqrt{\nu_e*})^2}, \qquad (15)$$

we obtain the solid line shown in Fig.1, which follows well the results obtained by CQL$_{//}$. We see that f_T^{eff} represents the effective fraction of trapped particles, which is reduced by collisions. Note that σ_{neo} for arbitrary collisionality was already obtained with CQL$_{//}$ by solving directly Eq.(1) with $v_D = 0$ [1].

In Fig.2, we show L_{31} vs ν_e* for ε=0.023. We see that CQL3D (solid circles) and Hirshman formula [5] (dashed-dotted line) give the same $\nu_e* \to 0$ limit for L_{31}, on the contrary to formulae of Refs.2 (dashed line) and 4 (dotted line). On the other hand, $L_{31}^{CQL//}$ (open circles) follows relatively well the latter formulae, valid for large collisionality.

In Fig.3, using the same labels as in Fig.2, we show the results obtained for $L_{31}/\sqrt{\varepsilon}$ for the same parameters as in Fig.1. First, for the banana limit ($\nu_e*=0$), we see that L_{31}^{CQL3D}

follows well Hirshman formula [5]. We have fitted the CQL3D results in terms of f_T and we obtain:

$$L_{31}^{CQL3D} = F_{31}(f_T) \equiv 1.62\, f_T - 0.84\, f_T^2 + 0.22\, f_T^3 \qquad (16)$$

This fit is represented by the crosses in Figs.2 and 3. Taking the same formula in terms of f_T^{eff} (solid line, Figs.2 and 3), we see that it reproduces well the results obtained with CQL$_{//}$ both versus ν_e^* (Fig.2) and ε (Fig.3). Therefore, we see that f_T^{eff} (Eq.(15)) does represent the effective fraction of trapped particles in the whole parameter domain (ε, ν_e^*). This enables us to have a simple analytical formula valid for the four limits: $\varepsilon \to 0$ / 1 and $\nu_e^* \to 0$ / ∞, and also for intermediate values of ε and ν_e^*. Note however that further studies for different tokamak equilibria and for very large ν_e^* are needed in order to better determine the dependence on $\sqrt{\nu_e^*}$ and ν_e^* of the denominator of Eq.(15).

In Fig.4 we show a contour plot of the adjoint function $\chi_e(v_{//}, v_\perp)$ for two cases shown in Fig.2: $\nu_e^*=0.04$ (Fig.4a) and $\nu_e^*=4$ (Fig.4b). As expected, we see that when the collisions are more important, the solution tends to a Maxwellian, independant of the pitch-angle, which reduces the effective trapped region. Moreover, this happens first in the low velocity region which explains why the coefficient L_{31}, proportional to $\chi_e\, v_{//} / v^3$, is more sensitive to ν_e^* than σ_{neo}, proportional to $\chi_e\, v_{//}$. This is seen by comparing Figs.1 and 3.

4. Conclusion

We have modified two codes, CQL3D and CQL$_{//}$, to solve the adjoint equation used to easily calculate the neoclassical conductivity and bootstrap current coefficients. In this way we can obtain these coefficients in banana and arbitrary collisionality regimes, respectively, for realistic axisymmetric tokamak equilibria. We have shown that the codes reproduce correctly the analytical formulae in the limits of small ν_e^* or small ε. We have also shown how CQL$_{//}$ is able to connect these limits for intermediate values of ν_e^* and ε, which enabled us to determine simple formulae for σ_{neo} and L_{31} in terms of an effective ratio of trapped particles (Eqs.(14-16)).

Acknowledgment

This work was supported in part by the Swiss National Science Foundation and by US-DOE contract Nos. DE-AC03-89ER51114, DE-AC02-76CH03073, and DE-AC05-84OR21400.

References

[1] O. Sauter, R. W. Harvey, and F. L. Hinton, Contrib. Plasma Physics **34** (1994) 169.
[2] F. L. Hinton and R. D. Hazeltine, Rev. Mod. Phys. **48** (1976) 239.
[3] S. P. Hirshman, R. J. Hawryluk, B. Birge, Nucl. Fus **17** (1977) 611.
[4] S. P. Hirshman, Phys. Fluids **21** (1978) 1295.

[5] S. P. Hirshman, Phys. Fluids **31** (1988) 3150.

[6] J. W. Connor, R. C. Grimm, R. J.Hastie, and P. M. Keeping, Nucl. Fus. **13** (1973) 211.

[7] J. Killeen, G.D. Kerbel, M.G. McCoy, and A.A. Mirin, "Computational Methods for Kinetic Models of Magnetically Confined Plasmas, Springer-Verlag, New York (1986) ; R.W. Harvey and M.G. McCoy, in Proc. IAEA TCM on Advances in Simulation and Modeling of Thermonuclear Plasmas, Montreal (1992).

[8] C. F. F. Karney, N. J. Fisch, and A. H. Reiman, in Proc. 8th Topical Conf. on RF Power in Plasma, Irvine (1989) (AIP), p. 430.

[9] S. P. Hirshman, K. C. Shaing, W. I. van Rij, C. O. Beasley, Jr., and E. C. Crume, Jr., Phys. Fluids **29** (1986) 2951.

[10] Y. R. Lin-Liu, F. L. Hinton, C. F. F. Karney, and S. P. Hirshman, in Proc. of the Int. Sherwood Fusion Theory Conf. (1994).

[11] S. P. Hirshman, Phys. Fluids **23** (1980) 1238.

[12] T. M. Antonsen, Jr., and K. R. Chu, Phys. Fluids **25** (1982) 129.

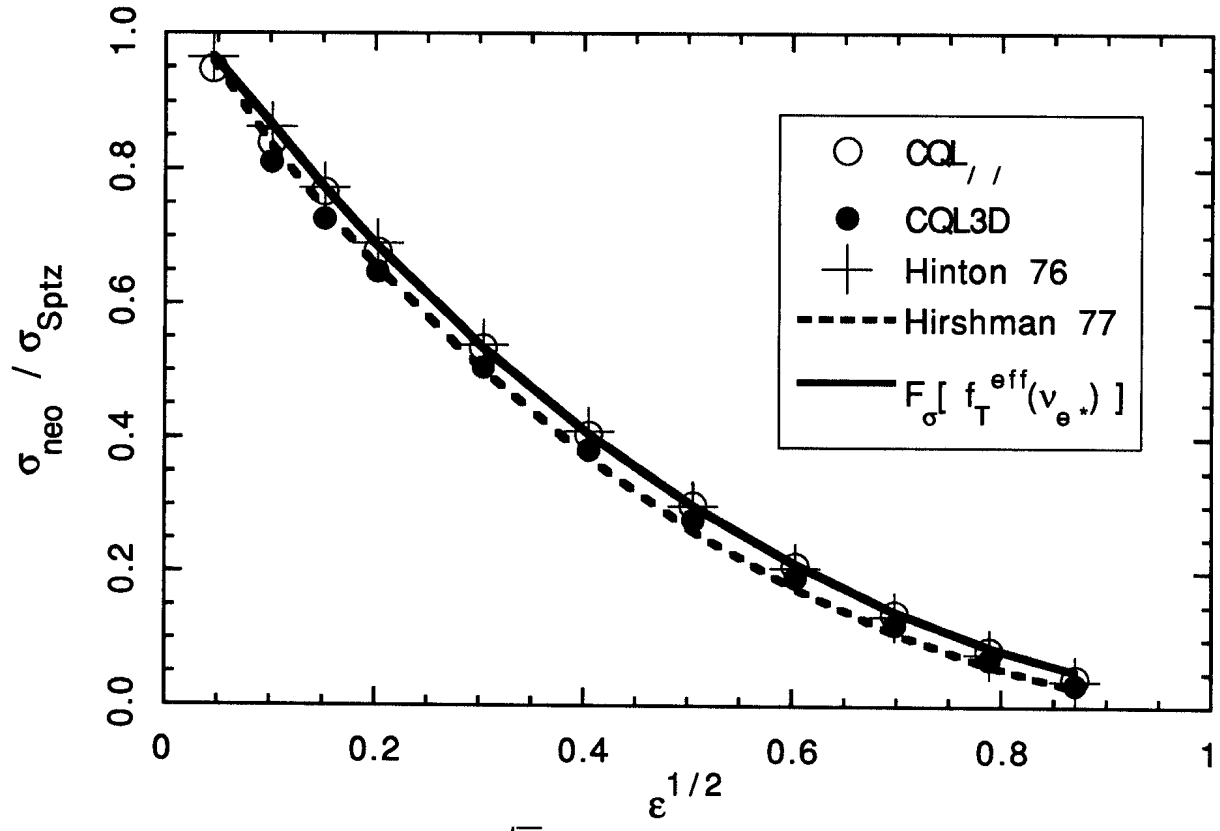

Fig.1: Neoclassical resistivity vs. $\sqrt{\varepsilon}$ with CQL$_{//}$ and CQL3D, compared with Hinton, Hirshman and Eqs.(14-15) formulae.

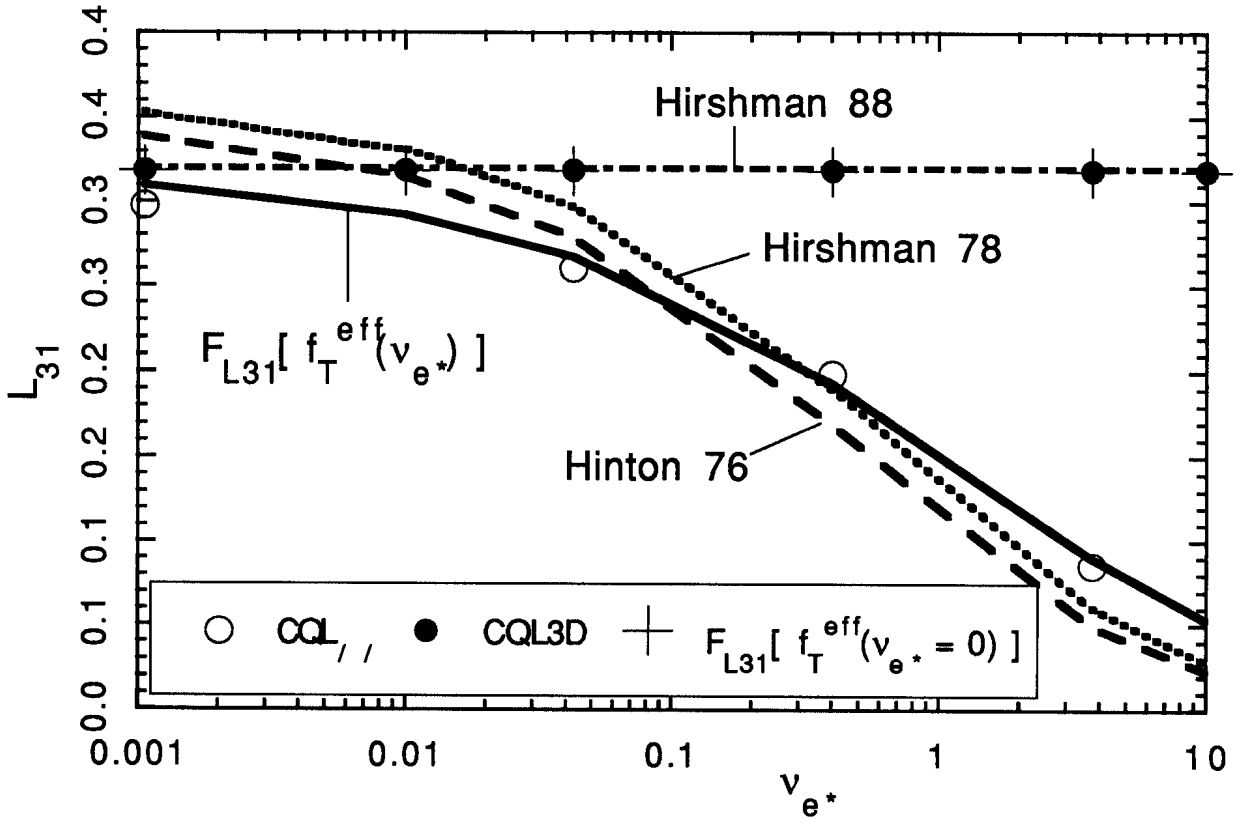

Fig.2: L_{31} vs. ν_{e*}, with ε=0.023, for CQL$_{//}$ (empty circles), CQL3D (solid circles), Eq.(16) (crosses) compared with Refs.[5] (dashed-dotted line), [2] (dashed line) and [4] (dotted line), and Eq.(15-16) (solid line).

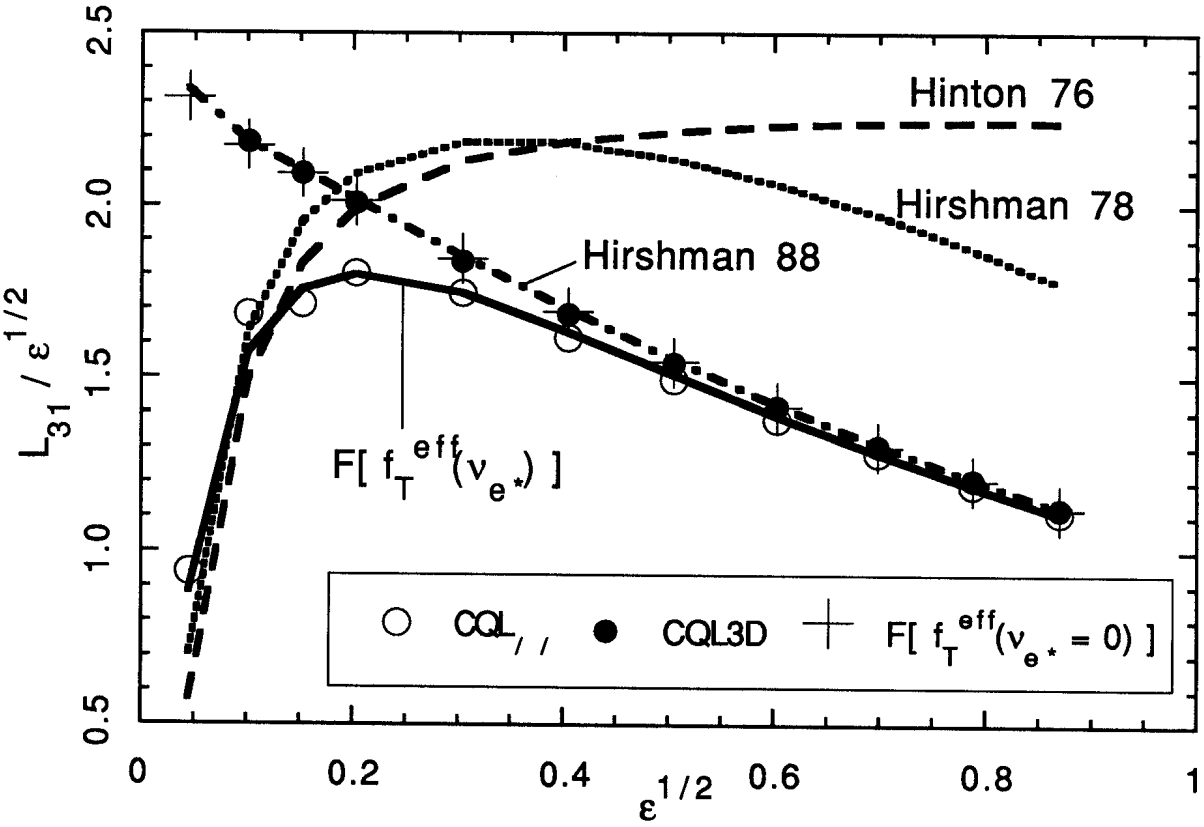

Fig.3: $L_{31}/\sqrt{\varepsilon}$ vs. $\sqrt{\varepsilon}$, with $n_e=10^{18}$ m^{-3} and T_e=3keV, with the same labels as in Fig.2.

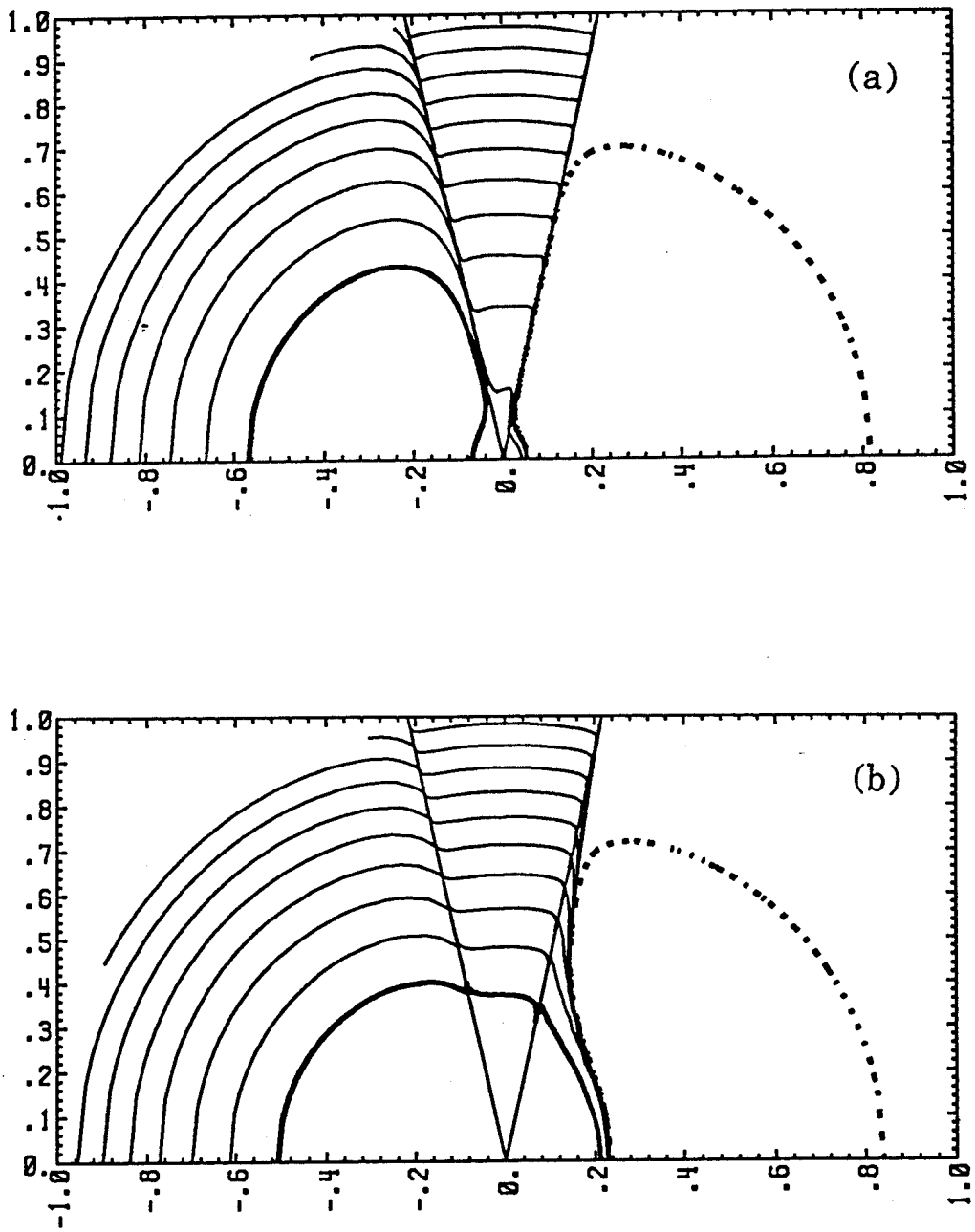

Fig.4: Contour plot of the adjoint function $\chi_e(v_{//}, v_\perp)$ for the cases with $\nu_e^*=0.04$ (a) and $\nu_e^*=4$ (b) shown in Fig.2. Only the contour for χ_e positive are drawn.